



Degree Project in Information and Network Engineering

Second cycle, 30 credits

# **The data-driven CyberSpine: Modeling the Epidural Electrical Stimulation using Finite Element Model and Artificial Neural Networks**

YU QIN



# **The data-driven CyberSpine: Modeling the Epidural Electrical Stimulation using Finite Element Model and Artificial Neural Networks**

YU QIN

Master's Programme, Information and Network Engineering, 120 credits  
Date: October 16, 2023

Supervisors: Grégory Dumont, Arvind Kumar, Grégoire Courtine  
Examiner: Jörg Conradt

School of Electrical Engineering and Computer Science

Host organization: .NeuroRestore(EPFL&CHUV)

Swedish title: Den datadrivna CyberSpine: Modellering Epidural Elektrisk  
Stimulering med hjälp av Finita Elementmodellen och Artificiella Neurala Nätverk



## Abstract

Every year, 250,000 people worldwide suffer a spinal cord injury (SCI) that leaves them with chronic paraplegia - permanent loss of ability to move their legs. SCI interrupts axons passing along the spinal cord, thereby isolating motor neurons from brain inputs. To date, there are no effective treatments that can reconnect these interrupted axons. In a recent breakthrough, NeuroRestore developed the STIMO neuroprosthesis that can restore walking after paralyzing SCI using Epidural Electrical Stimulation (EES) of the lumbar spinal cord. Yet, the calibration of EES requires highly trained personnel and a vast amount of time, and the mechanism by which EES restores movement is not fully understood. In this master thesis, we propose to address this issue using modeling combined with Artificial Neural Networks (ANNs). To do so, we introduce the CyberSpine model to predict EES-induced motor response. The implementation of the model relies on the construction of a multipolar basis of solution of the Poisson equation which is then coupled to an ANN trained against actual data of an implanted STIMO user. Furthermore, we show that our CyberSpine model is particularly well adapted to extract biologically relevant information regarding the efficient connectivity of the patient's spine. Finally, a user-friendly interactive visualization software is built.

## Keywords

Spinal Cord Injury, Epidural Electrical Stimulation, Computational Neuroscience, Finite Element Model, Artificial Intelligence, Optimal Transport, EMG, Muscle Activation



## Sammanfattning

Varje år drabbas 250 000 människor i hela världen av en ryggmärgsskada som ger dem kronisk paraplegi - permanent förlust av förmågan att röra benen. Vid en ryggmärgsskada bryts axonerna som passerar längs ryggmärgen, vilket isolerar de motoriska neuronpoolerna från hjärnans ingångar. Hittills finns det inga effektiva behandlingar som kan återansluta dessa avbrutna axoner. NeuroRestore utvecklade nyligen neuroprotesen STIMO som kan återställa gångförmågan efter förlamande ryggmärgsskada med hjälp av epidural elektrisk stimulering (EES) av ländryggmärgen. Kalibreringen av EES-stimuleringar kräver dock högutbildad personal och mycket tid, och den mekanism genom vilken EES återställer rörelse är inte helt klarlagd. I denna masteruppsats föreslår vi att vi tar itu med denna fråga med hjälp av modellering i kombination med artificiell intelligens. För att göra detta introducerar vi CyberSpine-modellen, en modell som kan förutsäga EES-inducerad motorisk respons. Implementeringen av modellen bygger på konstruktionen av en multipolär bas för lösning av Poisson-ekvationen som sedan kopplas till ett artificiellt neuralt nätverk som tränas mot faktiska data från en implanterad STIMO-deltagare. Dessutom visar vi att vår CyberSpine-modell är särskilt väl anpassad för att extrahera biologiskt relevant information om den effektiva anslutningen av patientens ryggrad. Slutligen bygger vi en användarvänlig interaktiv visualiseringsprogramvara.

## Nyckelord

Ryggmärgsskada, Epidural Elektrisk Stimulering, Beräkningsneurovetenskap, Finita Elementmodellen, Artificiell Intelligens, Optimal Transport, EMG, Muskelaktivering



## Acknowledgments

First and foremost, I would like to especially thank Dr. Grégory Dumont for his selfless help and patience in trying to teach me how proper science should be done and why life is meaningful.

I would like to thank Prof. Grégoire and Prof. Jocelyne for the parties we had and their great work done for the SCI patient to make all of these possibilities come true.

Huge thanks to Thibault Beineix for having so much encouragement through the 6 months and the suffering moments as well as the parties we have been through. Thanks to Alice, Pedro, Sergio, Icare (latent space expert), Xingchen, Alina, Hanane, Jonas, Nicolas, Robert, and Max, for having so much fun in CyberSpace and their valuable suggestions every day, also for the BBQ, hiking, shooting, archery, swimming, and badminton!

Thanks to but not limited to Gaia, Ruijia, Victor, Alan, Cathal, Robin, Henri, Nicolo, Thibault, Aasta, Charles, and Paula for the constructive conversations and the meetings we had. Thanks to Suzanne and Dylan for their help with the administration problems. I like the team.

Thanks to Prof. Arvind, for the passion for the science you delivered to us on the Neuroscience course and all the physical and mental support I got from you. I learned a lot from you.

Thanks to my high school friends Yitao and Xuxin. It is amazing we are still in the same city, all the way from Beijing to Lausanne.

Finally, thanks to my parents. Without their support, I can not achieve anything.

Stockholm, October 2023

Yu Qin



# Contents

|          |   |           |
|----------|---|-----------|
| <b>1</b> | <b>Introduction</b>   | <b>1</b>  |
| 1.1      | Overview . . . . .  | 1         |
| 1.2      | Background . . . . .  | 3         |
| 1.2.1    | Spinal Cord Neuroanatomy . . . . .                                      | 3         |
| 1.2.2    | Personalized spinal model for EES . . . . .                             | 7         |
| 1.2.3    | Deep learning Top-Down Approach for Neuroscience . . . . .              | 8         |
| 1.3      | Purpose and Problem . . . . .   | 9         |
| 1.3.1    | Computational Spinal Cord Model for EES . . . . .                       | 9         |
| 1.3.2    | Problem Definition . . . . .  | 9         |
| 1.4      | Research Methodology . . . . .  | 10        |
| 1.5      | Goals and Outcomes . . . . .  | 11        |
| 1.6      | Delimitation . . . . .  | 11        |
| <b>2</b> | <b>Methodology</b>  | <b>13</b> |
| 2.1      | Electromyography Data . . . . .   | 15        |
| 2.2      | Electroquasistatic Electromagnetic Simulation . . . . .                 | 16        |
| 2.3      | Multipolar Simulation . . . . .   | 17        |
| 2.4      | Cable Theory and Activation Function . . . . .                          | 20        |
| 2.5      | Artificial Neural Network Model of Root-Muscle Linkage . . . . .        | 21        |
| 2.6      | Validation Method . . . . .   | 23        |
| 2.7      | Optimal Transport Based Metric for Electrode Configurations . . . . .   | 24        |
| 2.8      | Software . . . . .  | 25        |
| <b>3</b> | <b>Results</b>  | <b>27</b> |
| 3.1      | FEM Result Visualization . . . . .                                      | 27        |
| 3.2      | Optimization of the Current Configuration for Root Activation . . . . . | 29        |
| 3.3      | Prediction of Muscle Activation . . . . .                               | 31        |
| 3.4      | Emergence of Myotome . . . . .  | 35        |

|          |   |           |
|----------|---|-----------|
| <b>4</b> | <b>Conclusions and Future work</b>        | <b>37</b> |
| 4.1      | Conclusions . . . . .                     | 37        |
| 4.2      | Limitations . . . . .                     | 38        |
| 4.3      | Future work . . . . .                     | 38        |
| 4.4      | Reflections . . . . .                     | 38        |
| 4.5      | Ethics . . . . .                          | 39        |
| 4.6      | Sustainability . . . . .                  | 39        |
|          | <b>List of Figures</b>                    | <b>43</b> |
|          | <b>List of Tables</b>                     | <b>45</b> |
|          | <b>List of acronyms and abbreviations</b> | <b>47</b> |
|          | <b>References</b>                         | <b>56</b> |

# Chapter 1

## Introduction

### 1.1 Overview

**Spinal Cord Injury (SCI)** refers to the impairment of any segment of the spinal cord, often leading to irreversible loss of physiological functions below the affected region [1]. The lesion resulting from SCI disrupts the transmission of electrical signals between the brain and the nervous system situated below the injury site. Consequently, patients may experience such as complete or incomplete paraplegia, significantly limiting their ability to walk. Over the past decades, **Epidural Electrical Stimulation (EES)** has been proved preclinically [2, 3, 4, 5, 6, 7, 8] and clinically [9, 10, 11, 12, 13, 14, 15, 16] as one potential solution to restore walking. EES is an invasive method, that requires surgery to position the electrode directly on the dura mater of the spinal cord. The EES rehabilitation equipment is shown in Figure 1.1.

More specifically, to restore walking, Spatiotemporal EES has proven to be an effective paradigm [6]. Spatiotemporal EES works by delivering specific stimulation patterns of EES according to the gait phase in order to activate different muscle groups with different functions. Gait can be divided into several key phases. Figure 1.2 illustrates the corresponding muscle activating during the certain gait phase, which is the pattern researchers want to reproduce through EES [15].

The EES clinical timeline is shown in Figure 1.3. The current configuration phase of EES relies on manual calibrations. Thus, using a computational model as prior knowledge holds the potential to automate the calibration procedure. After the rehabilitation, the patient is able to walk with the assistant equipment [9].

## 2 | Introduction

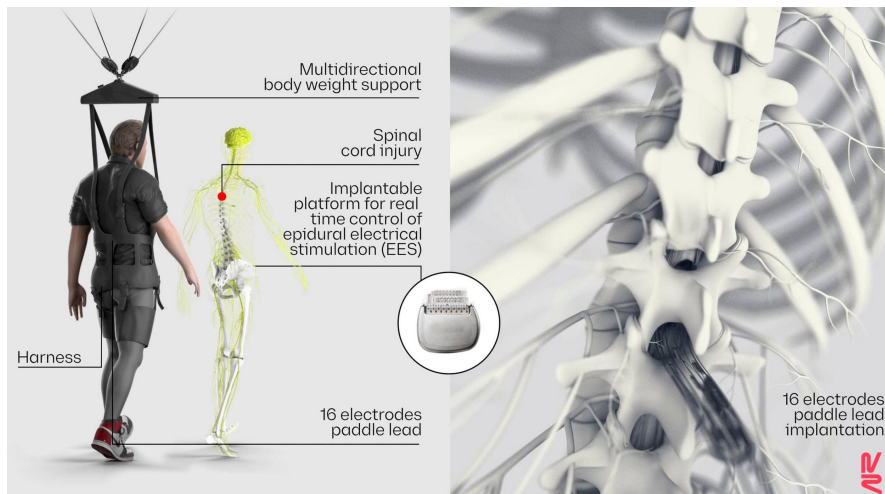


Figure 1.1: EES rehabilitation equipment. EES electrodes together with the body weight support equipment form one type of rehabilitation system aiming to help the patients walk. (Figure adapted from [17])

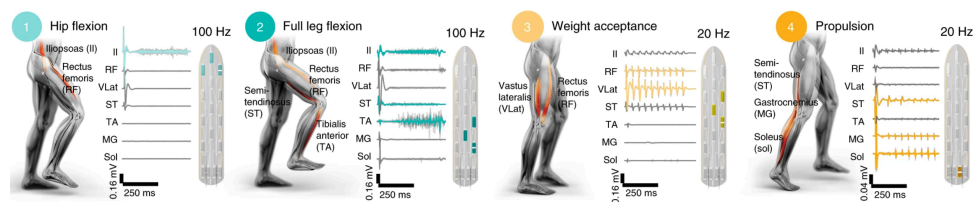


Figure 1.2: Ideal muscle activation through EES for key phases of gait. Electrodes alongside give examples of EES configurations for one specific patient to activate the corresponding muscle groups. (Figure adapted from [9])

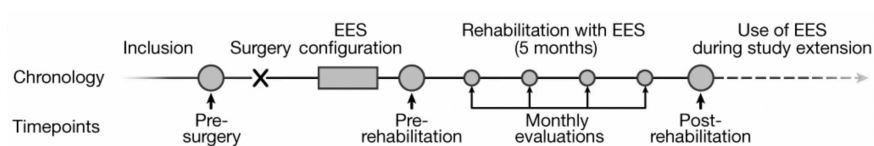


Figure 1.3: Typical EES clinical timeline. The whole procedure contains inclusion, surgery, EES configuration, rehabilitation with EES, and use of EES during study extension. (Figure adapted from [9])

## 1.2 Background

### 1.2.1 Spinal Cord Neuroanatomy

The **Central Nervous System (CNS)** comprises the brain and the spinal cord, as depicted in Figure 1.4, and the peripheral nervous system constitutes the other part of the nervous system. The spinal cord consists of various tissues, illustrated in Figure 1.5. The brain communicates information to the lower limb through the spinal cord. The SCI blocks this communication and causes paraplegia. For in-depth knowledge, one can refer to "Principles of Neural Science" [18].

The dorsal side of the spinal cord primarily contains ascending sensory pathways. These pathways transmit sensory information from the body to the brain, allowing us to perceive sensations such as touch, pain, temperature, and proprioception (awareness of body position). Conversely, the ventral side of the spinal cord primarily contains descending motor pathways. These pathways carry motor commands from the brain to the muscles, enabling voluntary movement and motor control throughout the body.

During our clinical trials, the EES electrode is positioned on the dorsal side of the spinal cord, exterior to the dura mater. Intuitively, one might assume that the ventral side would be a better choice for electrode placement, considering the presence of motor pathways in that region. However, there is evidence showing that preserving proprioception information over the dorsal side is also important to restore walking [11], and the dorsal side is easier to access during the surgery, compared to the ventral side.

In Figure 1.6, a detailed anatomic structure of the spinal cord is shown, including cervical (C), thoracic (T), lumbar (L), and sacral (S) segments. The EES targets the roots over lumbosacral segments to stimulate the walking-related muscles.

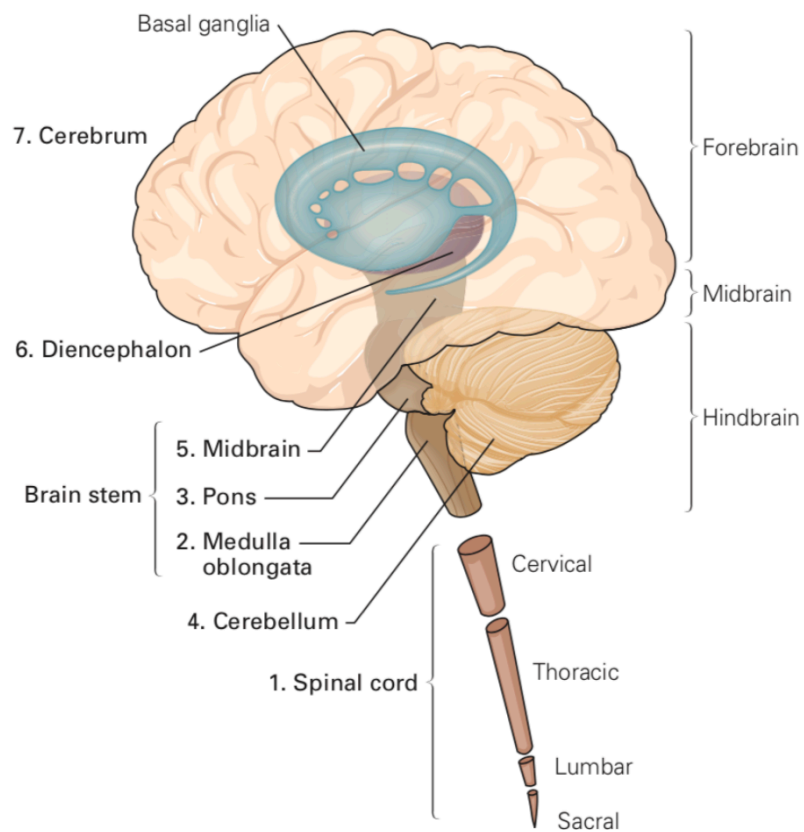


Figure 1.4: **CNS** anatomy. The spinal cord includes the cervical, thoracic, lumbar, and sacral segments. (Figure adapted from [18])

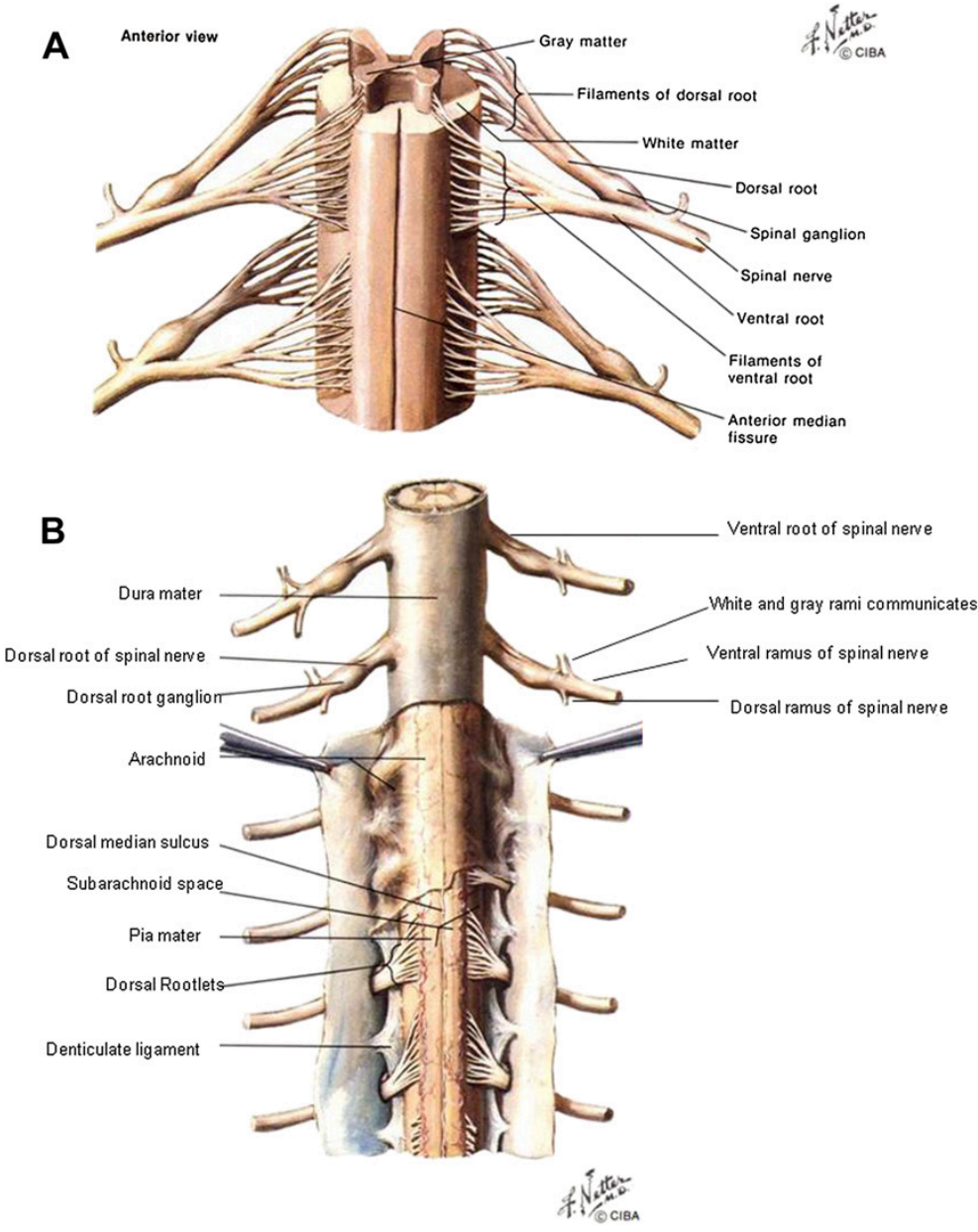


Figure 1.5: Anatomical structure of the spinal cord. (Figure adapted from [19])

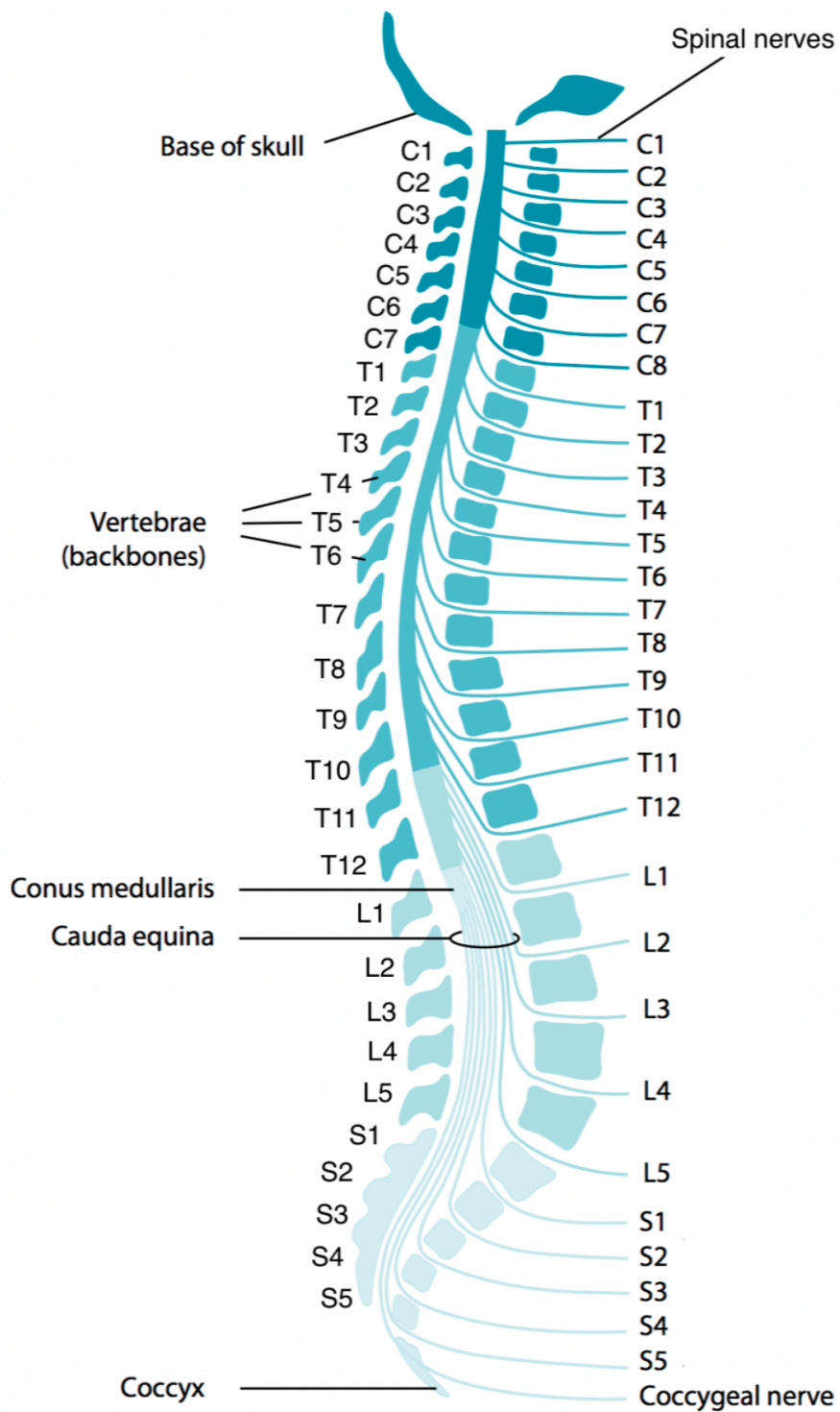


Figure 1.6: Division of the vertebrae along the spinal column, including cervical (C), thoracic (T), lumber (L), and sacral (S) segments. (Figure adapted from [1])

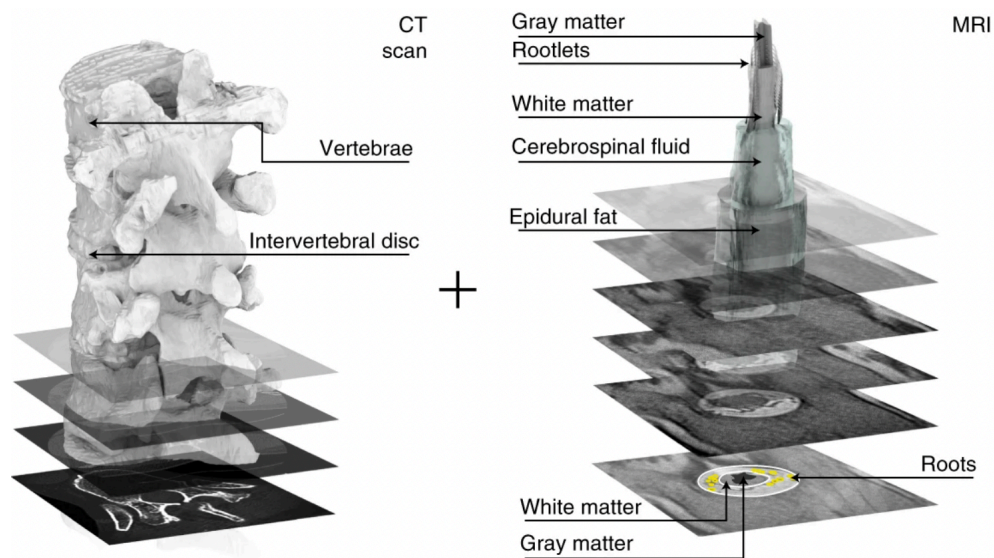


Figure 1.7: 3D personalized structural model built from CT scan MRI images. (Figure adapted from [9])

## 1.2.2 Personalized spinal model for EES

The detailed anatomical structures of the spinal cord exhibit variability among individuals [19]. This variability in the spinal cord requires the creation of personalized spinal models, ensuring the best possible therapeutic outcomes. These models are derived from high-resolution multimodal clinical images, combining data from Computerized Tomography (CT) and Magnetic Resonance Imaging (MRI) through a semi-automated process [9].

The output of the resulting algorithm provides the structural 3D model file containing all tissues shown in Figure 1.7 except the spinal roots, saving the x y z axes of each tissue's position and the name of the corresponding tissue. The segmentation of the spinal roots is done by hand. The spinal roots are crucial since the motivation of the simulation is to inspect the activation of the different roots, which will transmit the nerve impulse further to the muscles

In this thesis, the model provides the essential personalized structural file that will be used in the **Finite Element Model (FEM)**. It is worth mentioning that the model does not encompass all anatomical structures present in the spinal cord. Nevertheless, it does include most of the crucial tissues essential for calculating the electrical field distribution.

In Figure 1.8, the EES electrode placement and the relative position with the personalized spinal cord segments are shown.

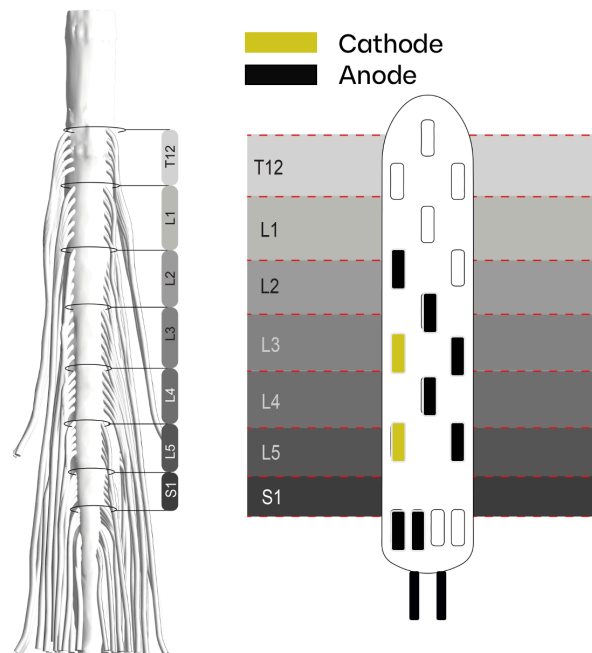


Figure 1.8: EES electrode placement and the relative position with the Spinal Segments with cathodes in yellow and anodes in black. In the figure, one configuration is shown and the activation of the roots should be around L3-L5.

### 1.2.3 Deep learning Top-Down Approach for Neuroscience

Deep learning has shown promising progress recently in building up artificial intelligent systems, thanks to the development of backpropagation optimization algorithm [20] and the ability to approximate functions with multilayer perceptron [21]. However, it is still controversial among different Neuroscience researchers how it could be used for scientific discovery. More specifically, Deep Learning builds up a model trying to predict the observations, without understanding the physical mechanism behind them from a foundationalism point of view—so-called the "Top-Down" Approach. Then, the model may reveal some hidden knowledge after the algorithm converges, but a proper way to connect this knowledge to the previous knowledge systems can not be found. There are papers suggesting this type of methodology [22, 23, 24].

In this thesis, we posit that the optimization-based model possesses the

potential to unveil latent information once it becomes proficient in predicting observed phenomena. This implies that once the model's outcomes converge, there is a likelihood that they provide insights into the underlying structure within the patient (if enough prior assumptions are imposed to the model).

## 1.3 Purpose and Problem

### 1.3.1 Computational Spinal Cord Model for EES

In section 1.1, we introduced the basic EES rehabilitation process. However, the underlying mechanism of how EES interacts with the neuronal system in the spinal cord remains unclear. To improve the rehabilitation's efficiency, it is essential to gain a clear understanding of the **Electromagnetism (EM)** phenomenon occurring inside the patient's spinal cord and the relation of the activation of spinal roots to the activation of muscles during EES.

Computational models help people understand better and perform scientific experiments when the research subject is too costly to perform experimental manipulation in the real world, by trying to capture the characteristics of the observed phenomenon. Then, a computational spinal cord model is a natural choice because of the fast, accurate result we can get from computer simulations and the boost of computer algorithms in the past decades. Previously, there were related models for electrical stimulation [25, 26, 27, 28, 29]. However, they are either not easily generalized or interpretable in multipolar situations. Modeling the stimulation over the spinal cord has been explored for decades. We refer to the [30] for a literature review of computational models for the design of spinal cord stimulation therapies.

### 1.3.2 Problem Definition

From previous works, several steps have already been achieved: the theory of constructing current-based multipolar EES simulation by setting monopolar simulations as a basis in linear space [25]; a program to optimize personalized voltage-based multipolar EES configuration given the target spinal root activation [31, 9]; the theory that neural network can be used to approximate functions [21].

Current-based multipolar EES allows the user to vary the current levels of individual electrodes for a more precise and targeted stimulation. This flexibility in current adjustments offers the potential to optimize the

therapeutic effects of the stimulation and tailor it to the patient's specific needs and condition.

One important problem during clinical trials is to decide which electrode configuration is proper to use for a certain muscle activation [9]. Then, with these achievements — Can we inspect the spinal root recruitment and predict the muscle activation with a prediction error of around 15% for each muscle given a certain EES configuration?

## 1.4 Research Methodology

The hypothesis throughout the thesis is that it is plausible to build a biophysical model that can predict muscle activation given current-based multipolar EES configurations over the spinal dorsal roots of the lumbosacral segments.

Operationalization for this hypothesis is to convert the muscle activation into **Electromyography (EMG)** signals. It is one way to observe muscle activation by acquiring the electric signal generated by muscle cells. The limitation of this operationalization is that the EMG sensor can only detect muscle activation from superficial muscles directly beneath the skin. However, it is a compatible choice for human patients because the EMG sensors are non-invasive.

This work is a continuation of the model [9]. In this paper, monopolar **FEM** simulation was provided but it did not predict the muscle activation.

There exists one similar work [29], which uses an end-to-end deep neural network to approximate biological systems from the spinal cord to muscles. This model predicts muscle activation based on EES parameters and optimizes EES parameters capable of producing desired EMG recruitment. However, the model does not provide inner information to explain which root is activated and does not inspect the EM field distribution along the spinal cord.

Here, we combine the work from the FEM simulation for EES [25, 9, 31] and inspiration from deep learning for neuroscience [22]. The methodology is a combination of bottom-up (FEM) and top-down (ANN) research approaches. First, FEM models the EM field distribution inside the lumbosacral spinal cord to gain detailed information from EES electrodes to spinal roots. Then, a biophysically interpretable **Artificial Neural Network (ANN)** is built to approximate the biophysical function mapping the EM field simulation results of the spinal roots to the muscle activation. The prediction of EMG is achieved by using the backpropagation algorithm [20] based on the patient's EMG dataset over the ANN.

## 1.5 Goals and Outcomes

The goal of this project is to get a biophysical computational model of the spinal cord to simulate the effect of EES, combining the quasistatic electromagnetism FEM with an ANN. This has been divided into the following three sub-goals:

1. Prediction of the spinal root activation percentage or the muscle activation percentage given the input current-based multipolar EES configurations;
2. Optimization algorithm of the electrode setup given a root activation target;
3. Interactive Visualization Software for checking the EM field simulation results of current-based multipolar EES.

The outcomes of this thesis are the following:

1. Sub-Goal 1, 2, 3 are achieved;
2. The myotome matrix of the patient emerged from the neural network as a secondary result of the prediction;
3. An **Optimal Transport (OT)** based metric to measure the distance between two electrode configurations is provided.

## 1.6 Delimitation

This work only validates the personalized model over the spinal lumbosacral segments. The model is simplified by excluding unimportant physiological factors related to EM properties.

In the thesis, only an optimization algorithm for targeted root activation is implemented. There is no experiment related to optimization toward targeted EMG activation.

The biophysical model is not fully deductively generated. It remains an open discussion whether the phenomenal neuroscience model generated from the top-down approach is interpretable or not [22].



## Chapter 2

# Methodology

The overall methodological workflow is shown in Figure 2.1. To achieve the goal of the thesis, we would import a personalized model built from CT/MRI, to further perform FEM analysis on it. The Activation Function is then calculated, and together with the output of the FEM, to be the input of the ANN, to predict the final muscle activation generated from the previously collected EMG dataset.

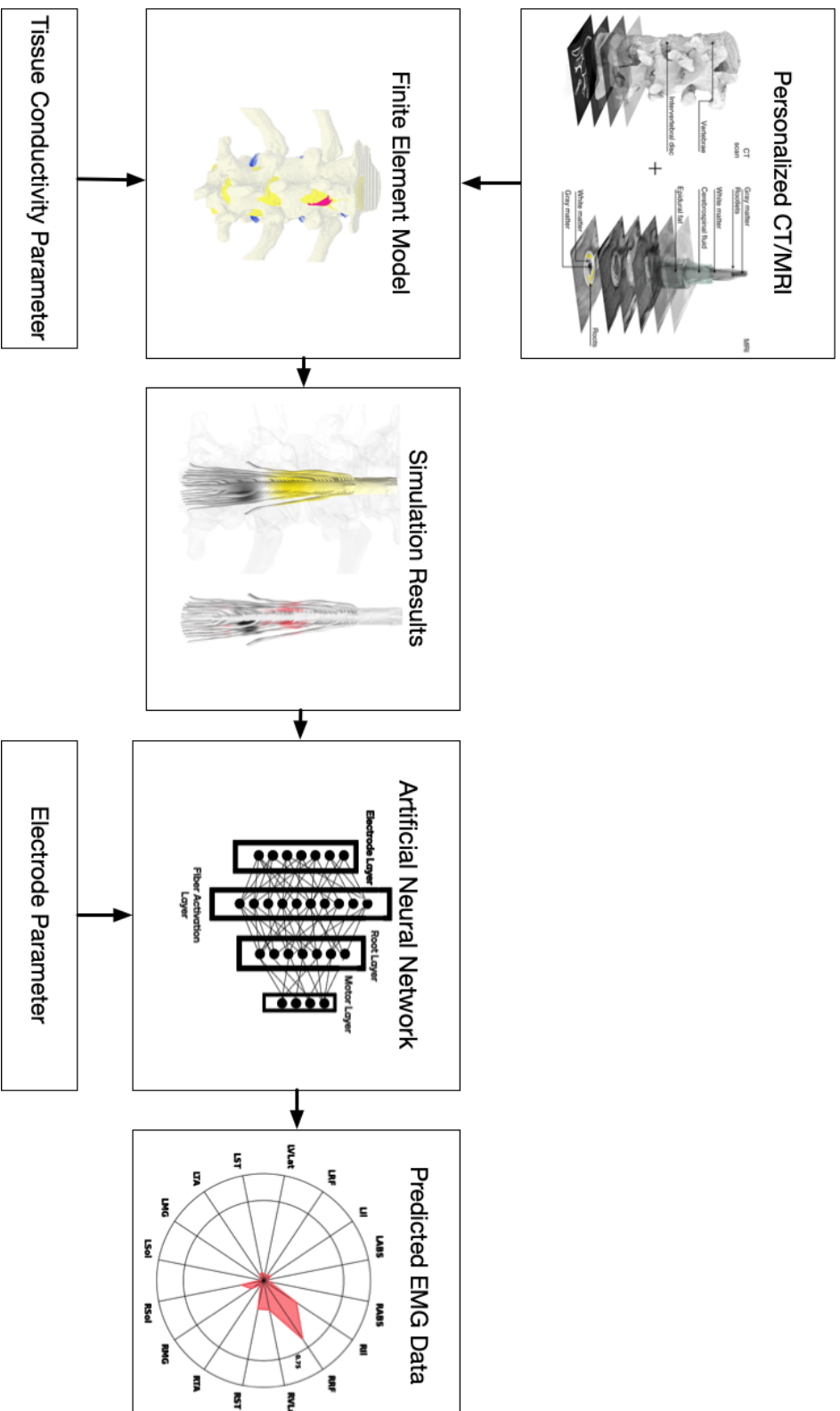


Figure 2.1: Workflow of the project. The Finite Element Model (FEM) takes the anatomical model and the tissue conductivity as given. Then, after performing Electroquasistatic Electromagnetic Simulation, the basis of the solutions to performed multipolar simulations is stored and used as input of the ANN. Taking any electrode configurations, the ANN calculates the Activation Function and trains to output EMG data.

## 2.1 Electromyography Data

The STIMO dataset was acquired during the use of the STIMO neuroprostheses by the STIMO clinical trial (www.clinicaltrials.gov ID NCT02936453) participants with chronic paraplegia secondary to spinal cord injury. The STIMO dataset includes fully characterized recordings of motor patterns evoked by EES protocols of varying parameters: configuration of electrodes that deliver EES, EES frequency, amplitude, and duration. The recordings comprise **EMG** of all major leg muscles of both legs. The EMGs were recorded by the experimentalists Gaia Carparelli and Pedro Abranches at a sampling frequency of  $1259.25\text{ Hz}$ , an example is shown in Figure 2.2.

Preprocessing the EMG data into "Muscle Activation" is done by dividing the maximum activation of the single trial of one particular muscle by the maximum activation of this muscle across the whole session. The calculation is based on the EMG data in the last half period of time of the stimulation to account only for the stationary activation of the muscle. Then the muscle activation converts into the percentage of activation. Thus, the data is normalized based on the maximum value of the session as the maximum to avoid shifting between sessions.

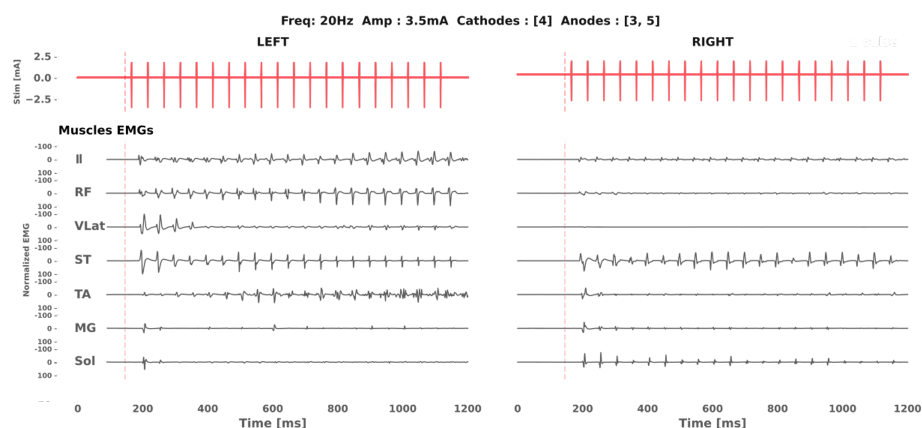


Figure 2.2: An example of one trial of EMG data. The EES is set to 20Hz and 3.5mA, with electrodes No.4 as the cathode and electrodes No.3 and 5 as anodes. The left and right refer to the left and right lower limbs. The figure is plotted within the time domain. The red line represents the pulses of EES. Iliacus(IL), Rectus Femoris (RF), Vastus Lateralis (Vlat), Sartorius (ST), Tibialis Anterior (TA), Gastrocnemius Medialis (MG), and Soleus (Sol) EMG signals are shown here.

## 2.2 Electroquasistatic Electromagnetic Simulation

Quasi-static EM simulation is based on one simplification of Maxwell's equations where the electrical field is considered to change slowly. In doing so, the time derivative can be ignored in the calculation. Computation resources and complexity decrease significantly with this simplification. The set of Maxwell's equations is:

$$\begin{cases} \nabla \cdot \mathbf{E} = \frac{\rho}{\epsilon_0} \\ \nabla \cdot \mathbf{B} = 0 \\ \nabla \times \mathbf{E} = -\frac{\partial \mathbf{B}}{\partial t} \approx 0 \\ \nabla \times \mathbf{B} = \mu_0 \left( \mathbf{J} + \epsilon_0 \frac{\partial \mathbf{E}}{\partial t} \right). \end{cases} \quad (2.1)$$

Here,  $\mathbf{E}$  represents the electric field, and  $\mathbf{B}$  represents the magnetic field. The desired outcome pertains to the electrical potential  $V$ . With electroquasistatic assumption, it follows that

$$\mathbf{E} = -\nabla V.$$

Then, after algebraic manipulations [25], the problem at hand simplifies to Poisson's equation:

$$\nabla \cdot (\sigma(\mathbf{x}) \nabla V(\mathbf{x})) = 0, \quad (2.2)$$

where  $\sigma(\mathbf{x})$  is the conductivity of the physiological tissues.

To establish a well-defined partial differential equation, one must specify appropriate boundary conditions for Equation 2.2. Boundary conditions determine how the electric potential  $V(\mathbf{x})$  behaves on the boundaries of the domain in consideration. These conditions are crucial in defining a unique solution for the partial differential equation. In our case, if the computation domain  $\Omega$  is set in voltage as

$$V(\mathbf{x}) = v_0(\mathbf{x}), \forall \mathbf{x} \in \partial\Omega \quad (2.3)$$

with  $v_0 : \mathbb{R}^n \rightarrow \mathbb{R}$ , it is named Dirichlet boundary condition. If the boundary  $\Omega$  is set in current density  $j_0$  as

$$\sigma(\mathbf{x}) \nabla V(\mathbf{x}) \cdot \mathbf{n}(\mathbf{x}) = j_0(\mathbf{x}), \forall \mathbf{x} \in \partial\Omega \quad (2.4)$$

| Tissue              | Conductivity (S/m) |
|---------------------|--------------------|
| Gray Matter         | 0.23               |
| Bone                | 0.02               |
| Disc                | 0.65               |
| Fat                 | 0.04               |
| Cerebrospinal Fluid | 0.65               |
| Paddle              | 1e-12              |
| Saline              | 2.0                |

Table 2.1: Conductivity Parameters

with  $j_0 : \mathfrak{R}^n \rightarrow \mathfrak{R}$ , it is named Neumann boundary condition.

In clinical situation for our EES electrodes, implanted electrodes are set in current  $I$ , named **Integrated Current Condition (ICC)**, where

$$\int_{\Omega} \sigma(\mathbf{x}) \nabla V(\mathbf{x}) \cdot \mathbf{n}(\mathbf{x}) ds = I_0. \quad (2.5)$$

The condition means the integration of the current density over the surface of  $\Omega$  is equal to the current value one set in the practical situation.

FEM solvers tackle the problem by discretizing equations and using numerical algorithms. Commercial software Sim4life is used in our case. The structural model and the model after voxelization in Sim4Life are shown in Figure 2.3. The conductivity of different tissues is obtained from [27], listed in Table 2.1.

## 2.3 Multipolar Simulation

One important property of Maxwell's equations and the simplified Poisson's equation is to be linear. Thus, a set of linearly independent solutions to the equations could form a basis that can span the whole solution space. To make multipolar EES simulations, we only need to solve certain numbers of linearly independent conditions.

The Sim4Life software used to solve Poisson's equation can only set Dirichlet boundary conditions, which form the solution for voltage-controlled multipolar configurations. Thus, we need an algorithm to convert the solution from the accessible Dirichlet condition into the ICC. Defining:

- $\{T_i\}_{i=0,1,\dots,N-1}$  represents the set of  $n$  electrodes

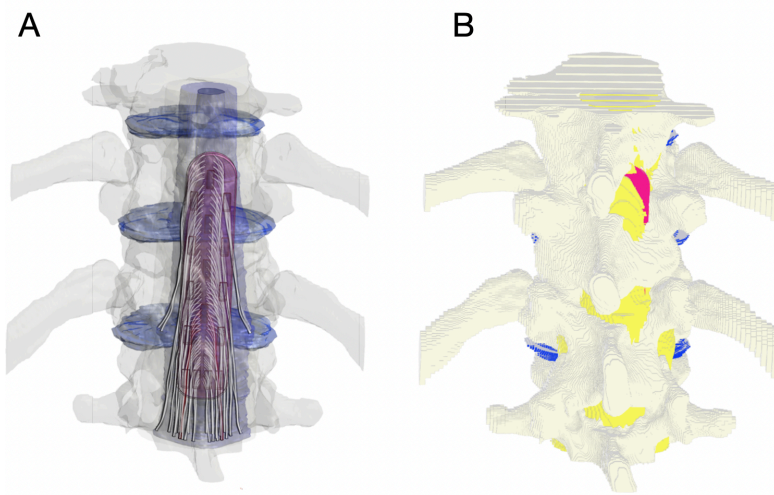


Figure 2.3: Anatomical model and its associated Finite Element model. A: Outlook of the anatomical model. The model includes bones, discs, white matter, spinal roots, and EES paddles. B: The figure displays the resulting finite element model obtained after the voxelisation of the anatomical model.

- $\Omega$  represents the whole spinal cord model where we would perform electroquasistatic simulations
- $\partial\Omega$  represents the boundaries including the outer edge of the simulation area plus the electrodes
- $\{v_i\}$  represents one group of linearly independent boundary conditions, for instance,  $\{v_i\} = \{1, 0, 0, \dots, 0\}$ ,

then the voltage-controlled multipolar configurations, which has Dirichlet boundary 2.3 over  $\{T_i\}$  (solved with Sim4life), reads

$$\begin{cases} \nabla \cdot (\sigma(\mathbf{x})\nabla V(\mathbf{x})) = 0 & \forall \mathbf{x} \in \Omega \\ \sigma(\mathbf{x})\nabla V(\mathbf{x}) \cdot \mathbf{n}(\mathbf{x}) = 0 & \forall \mathbf{x} \in \partial\Omega/\{T_i\} \\ V(\mathbf{x}) = v_i & \forall \mathbf{x} \in \{T_i\}. \end{cases} \quad (2.6)$$

The current-controlled multipolar configurations, which has ICC 2.5 over

$\{T_i\}$ , stated as

$$\begin{cases} \nabla \cdot (\sigma(\mathbf{x})\nabla V(\mathbf{x})) = 0 & \forall \mathbf{x} \in \Omega \\ \sigma(\mathbf{x})\nabla V(\mathbf{x}) \cdot \mathbf{n}(\mathbf{x}) = 0 & \forall \mathbf{x} \in \partial\Omega/\{T_i\} \\ \int_{T_i} \sigma(\mathbf{x})\nabla V(\mathbf{x}) \cdot \mathbf{n}(\mathbf{x}) ds = I_i & \forall \mathbf{x} \in \{T_i\}. \end{cases} \quad (2.7)$$

Thanks to the inspiration from [25] and Esra Neufeld for providing a linear operator to transform the basis from the space of voltage-controlled configurations to current-controlled multipolar configurations.

Making use of the linear property of the equation, one can find a basis that can span all possible solutions for the simplified Poisson's equation, noted as

$$V(\mathbf{x}) = \sum_i v_i V_i(\mathbf{x}), v_i \in \mathfrak{R} \quad (2.8)$$

where  $V_i(\mathbf{x})$  represents one simulation result as an eigenvector of the whole solution space.

Due to the gauge constant, the degree of freedom of the solution space for voltage potential is  $N - 1$ , where  $N$  is the number of electrodes in our case. For a detailed explanation, one should check the mathematical proof in [25]. Then, we can assume  $v_0 = 0$ . By the linearity of the gradient operator and of the integral, we could obtain

$$\int_{T_j} \sigma(\mathbf{x})\nabla V(\mathbf{x}) \cdot \mathbf{n}(\mathbf{x}) ds = \sum_{i \geq 1}^{N-1} v_i \int_{T_j} \sigma(\mathbf{x})\nabla V_i(\mathbf{x}) \cdot \mathbf{n}(\mathbf{x}) ds. \quad (2.9)$$

Denoting

$$I_{ij} := \int_{T_j} \sigma(\mathbf{x})\nabla V_i(\mathbf{x}) \cdot \mathbf{n}(\mathbf{x}) ds,$$

then, it is easily obtained that

$$I_j = \sum_{i \geq 1}^{N-1} v_i I_{ij} \quad \forall j = 1, 2, \dots, N$$

If we define the matrix  $\mathbf{J}$ , vectors  $\mathbf{I}$  and  $\mathbf{V}$  as

$$\mathbf{J} := (I_{ij})_{1 \leq i, j \leq N-1}^T := \begin{pmatrix} I_{11} & I_{21} & \cdots & \cdots & I_{N-11} \\ I_{12} & I_{22} & \cdots & \cdots & I_{N-12} \\ \vdots & \vdots & \ddots & & \vdots \\ \vdots & \vdots & & \ddots & \vdots \\ I_{1N-1} & I_{2N-1} & \cdots & \cdots & I_{N-1N-1} \end{pmatrix}$$

and

$$\mathbf{I} := \begin{pmatrix} I_1 \\ I_2 \\ \vdots \\ \vdots \\ I_{N-1} \end{pmatrix} \quad \mathbf{V} := \begin{pmatrix} v_1 \\ v_2 \\ \vdots \\ \vdots \\ v_{N-1} \end{pmatrix},$$

then, we would obtain

$$\mathbf{V} = \mathbf{J}^{-1}\mathbf{I}. \quad (2.10)$$

With the formula, the wanted coefficients in current  $\mathbf{I}$  can be converted into the equivalent coefficients in voltage  $\mathbf{V}$ . The matrix  $\mathbf{J}$  is obtained by integrating the current density over the electrodes  $T_i$  with the simulation  $j$  under the Dirichlet boundary condition. It is worth noting that, due to the gauge constant, the

$$I_0 = 0 - \sum_{i \geq 1}^{N-1} I_i, \quad v_0 = 0.$$

Finally, the value over  $N$  electrodes was transformed from the given current value to the voltage value, which solves our problem by converting the accessible simulation results of voltage-controlled configurations in Sim4Life to the current-controlled multipolar configurations.

## 2.4 Cable Theory and Activation Function

To predict muscle activation, knowledge of the activation of the spinal roots is needed. In Computational Neuroscience, the cable theory is used to biophysically model the transmission process of electrical signals along the nerve fibers (also named axons). The gold standard cable model for electrical

stimulation is the Spatially Extended Nonlinear Node (SENN) [32], given as

$$C_m \frac{dV_n}{dt} + I_{e,n} = G_a (V_{e,n-1} - 2V_{e,n} + V_{e,n+1}). \quad (2.11)$$

In this equation,  $C_m$  is the membrane capacitance,  $\frac{dV_n}{dt}$  represents the time derivative of the membrane voltage  $V_n$ ,  $I_{e,n}$  is the current injected at node  $n$  of segment  $i$ , and  $G_a$  is the axial conductance. The SENN model accounts for the spatial and temporal dynamics of the electrical stimulation response in an axon, making it a reliable benchmark for assessing the effectiveness of electrical stimulation paradigms.

However, SENN becomes computationally burdensome when applied to large-scale simulations. In [31], another method has been proposed based on a simpler method: the **Activation Function (AF)** method.

Knowing the electric potential  $V(\mathbf{x})$  along the spinal cord model, the activation function [31], which is a normalized version of the induced current along the neuro fibers, can be used to calculate the activation of the nerves.

The AF assumes the external current is dominant so that the internal current can be ignored and excluding the temporal calculation., given as

$$\begin{aligned} \frac{dV_n}{dt} &\approx AF_n = \frac{G_a}{C_m} (V_{e,n-1} - 2V_{e,n} + V_{e,n+1}) \\ &= \frac{d\Delta x}{4\rho l c_m} \cdot \frac{V_{e,n-1} - 2V_{e,n} + V_{e,n+1}}{\Delta x^2}. \end{aligned} \quad (2.12)$$

In practice, the first term can be seen as a constant, which does not affect our calculation and can be set to 1. The AF employs the second derivative of electrical potentials to depict the driving force behind nerve impulses. In practice, when examining a single neuron fiber, if the AF surpasses the neuron's membrane potential, it is considered an action potential, implying that the fiber has been activated.

Then, one can get the root activation of the spinal roots based on the AF formula, which is necessary to construct ANN later.

## 2.5 Artificial Neural Network Model of Root-Muscle Linkage

In Section 1.2.3, we introduced the assumption of using a "Top-Down" approach and to leverage an Artificial Neural Network as a tool to answer

Neuroscience related questions. Here, we describe the network in charge of predicting EES-induced motor activation.

First, we name the calculation of the EM field from the multipolar simulation results given a certain electrode configuration as the "Electrode Layer". Then, we denote

$$\vec{AF}_{r,f} = (AF_{r,f}^0, AF_{r,f}^1, \dots, AF_{r,f}^{n-1})$$

the activation function of the nerve fiber  $f$  belonging to the root  $r$ , each  $AF_{r,f}^i$  is calculated according to 2.12. We can then determine if the nerve fiber is active. We define the "Fiber Activation Layer":

$$A_{r,f} := \begin{cases} 0 & \text{not active} \\ 1 & \text{active} \end{cases} = H\left(\frac{Th_{r,f} - \max(\vec{AF})}{\gamma}\right) \quad (2.13)$$

with  $Th_{r,f}$  representing the fiber threshold and  $H$  representing the Heaviside function. In practice, since  $H$  is not differentiable, it is replaced by a sigmoid function and  $\gamma$  is a scaling factor to approximate  $H$ . Then, for a given root, we define the spinal root activity as the percentage of the activated fibers, named "Root Layer":

$$R_r := \frac{1}{N_f} \sum_{f=0}^{N_f-1} A_{r,f}. \quad (2.14)$$

We define the calculation of the muscle activity of muscle  $m$  as the "Motor Layer":

$$M_m := \sigma\left(\frac{1}{N_r} \sum_{r=0}^{N_r-1} |J_{m,r}| R_r\right), \quad (2.15)$$

with  $J_{m,r}$  representing the coefficient of the myotome matrix between which links root  $r$  to muscle  $m$ .

Since the electrode is placed on the dorsal side of the root, to activate the muscles, which are controlled by the motor neuron on the ventral side of the spinal cord, EES will recruit spinal interneurons. Then, we assume the  $\sigma$  as a non-linear function could describe the non-linearity of the relationship between the dorsal roots and the muscle. For interest, Equation 2.15 denotes a static simplified version of the Wilson-Cowan Model [33].

In one clinical trial, only one type of electrode configuration will be implemented. For one trial, we have  $N_m$  Muscle Activation data  $M$ . The

loss function is defined as

$$\mathcal{L}_{trial}(Th, J) := \frac{1}{N_m} \sum_{m=0}^{N_m-1} (M_m - \hat{M}_m)^2. \quad (2.16)$$

Consequently, the goal of the ANN is to

$$\min_{Th, J} \sum_{trail=0}^{N_{trail}-1} \mathcal{L}_{trial}(Th, J). \quad (2.17)$$

In this shallow ANN, the only trainable parameters are the thresholds of different nerve fibers  $Th$  and the myotome weight matrix  $J$ .

In the above definitions, all mathematical operations can be implemented within Pytorch and the optimization problem is solved using backpropagation. The parameters are listed here:

- Dataset:  $N_f = 50$ ,  $N_r = 20$ ,  $N_m = 16$ ,  $N_{trail} = 669$ .
- Epochs: 2000.
- Learning Rate: 0.25.
- Optimizer: Adam.
- Initialization of the Threshold  $Th$  per fiber (same for all roots): [9200, 8710, 8239, 7740, 7250, 6760, 6280, 5790, 5300, 4810] replicated by 5 times. Values are adopted from results generated from Neuron Simulations in [31].
- $\gamma$ : The standard deviation divided by 2 of the initialized thresholds.
- Initialization of the weight matrix  $J$ : Xavier uniform initialization with gain equals 10.

## 2.6 Validation Method

To validate computational model predictions, we took advantage of the data recorded under the STIMO clinical trial. We used 20 percent of the recorded sessions that map EMG responses to complex and unseen EES protocols. We compared predictions made by the personalized computational model and the recording from the mapping sessions. We considered the model to be validated if the mean absolute error in muscle activation is below 15 percent.

While aiming for the weight matrix  $J$  to converge, our goal is to achieve biophysical interpretability, enabling it to reflect the true myotome of a patient. Ideally, the matrix should be validated through anatomical examination of the patient. However, in our specific scenario, conducting such validation via surgery on the patient is unrealistic.

We could know the myotome should follow some order from the previous studies [9, 34, 35, 36, 36, 37]. Researchers agree there should be an order of muscle connecting to different roots, but patient-to-patient variability exists. Thus, the only way to validate how large the chance that the matrix we get could be true is to check whether the myotome can show some kind of "diagonal" tendency once we sort the muscle and the root according to the common agreement.

## 2.7 Optimal Transport Based Metric for Electrode Configurations

Lastly, we define an Optimal Transport based metric for electrode configurations to measure the distance between two electrodes. The metric is not used in this thesis but would be useful for future work.

With the assumption that the current flowing out of an electrode can be simplified as a flow of charge over a point, we denote one electrode configuration as

$$E = \sum_{i=1}^N q_i \delta(e - e_i),$$

where  $e_j$  represents the coordination of the electrode  $i$  in the Euclidean space and  $q_j$  represents the amount of charge flowing out the electrode  $i$ . Assuming  $N$  electrode contacts on the electrode array, we assume

$$q_i \in [-1, 1], \forall i = 1, 2, \dots, N, \sum_{i=1}^N q_i = 0.$$

We separate cathodes as

$$c_i = \begin{cases} -q_i & \text{if } q_i < 0 \\ 0 & \text{otherwise} \end{cases} \quad (2.18)$$

with

$$C = \sum_{i=1}^N c_i \delta(e - e_i),$$

and anodes as

$$a_i = \begin{cases} q_i & \text{if } q_i \geq 0 \\ 0 & \text{otherwise} \end{cases} \quad (2.19)$$

with

$$A = \sum_{i=1}^N a_i \delta(e - e_i).$$

Then we get

$$\begin{aligned} E &= \sum_{i=1}^N q_i \delta(e - e_i) \\ &= C + A. \end{aligned} \quad (2.20)$$

Finally, we define the distance between two electrodes  $E$  and  $E'$  as the following:

$$d(E, E') := W_2(C, C') + \alpha W_2(A, A') \quad \alpha > 0, \quad (2.21)$$

where  $W_2$  represents the Wasserstein distance in the Euclidean space. Since the place of cathodes is more determinant regarding the EM field property,  $\alpha$  is a control parameter to adjust how important the anodes are.

## 2.8 Software

All along this thesis, we have used the following software: Sim4Life V 7.0.1.8169 is used for the **FEM** simulation; Python 3.6.13, Numpy 1.16.6, and Torch 2.0.1+cu117 are used for calculating **AF**, building **ANN** and predicting the muscle activation. Mayavi 4.8.1 is used for visualization.



# Chapter 3

## Results

### 3.1 FEM Result Visualization

The personalized computational model is a tailor-made model of the patient's spine. It consists of a 3-dimensional volume conductor providing access to the anatomical structure of the patient's spine. This is made possible by a tissue segmentation of high-resolution MRI scans of the patient's spine. The resulting CyberSpine of the patient includes vertebra, discs, fatty layer, cerebrospinal fluid, white matter, and accurate trajectory of spinal roots. Assignment of the tissue conductivity allows the calculation of stimulation-induced electrical field generated by EES for a given electrode array configuration (i.e. electrode shape, active site, electrode polarity, ...).

To construct a multipolar basis of solutions, we conducted 15 simulations of voltage-controlled EES. Each simulation involves linearly dependent vectors  $v_i$ , as outlined in Equation 2.6. Subsequently, the resulting EM field distribution was converted into current-controlled multipolar EES using Equation 2.10. Then, one can set arbitrary values in  $\mathbf{I}$  (sum needs to be 0) and obtain the corresponding EM solution for any electrode configuration.

By implementing the methodology, we then need ways to first inspect whether the simulation results are coherent with common sense or not, which means the current should follow from cathodes to anodes, as well as the electrical distribution should be gradually changed from cathodes to anodes, should be observed from the model. Thus, we will provide the visualization of the computational results generated from the Finite Element Model simulation and the Activation Function as a way to obtain a first impression of the stimulation effect.

In Figure 3.1, we display the resulting EES simulation for two electrode

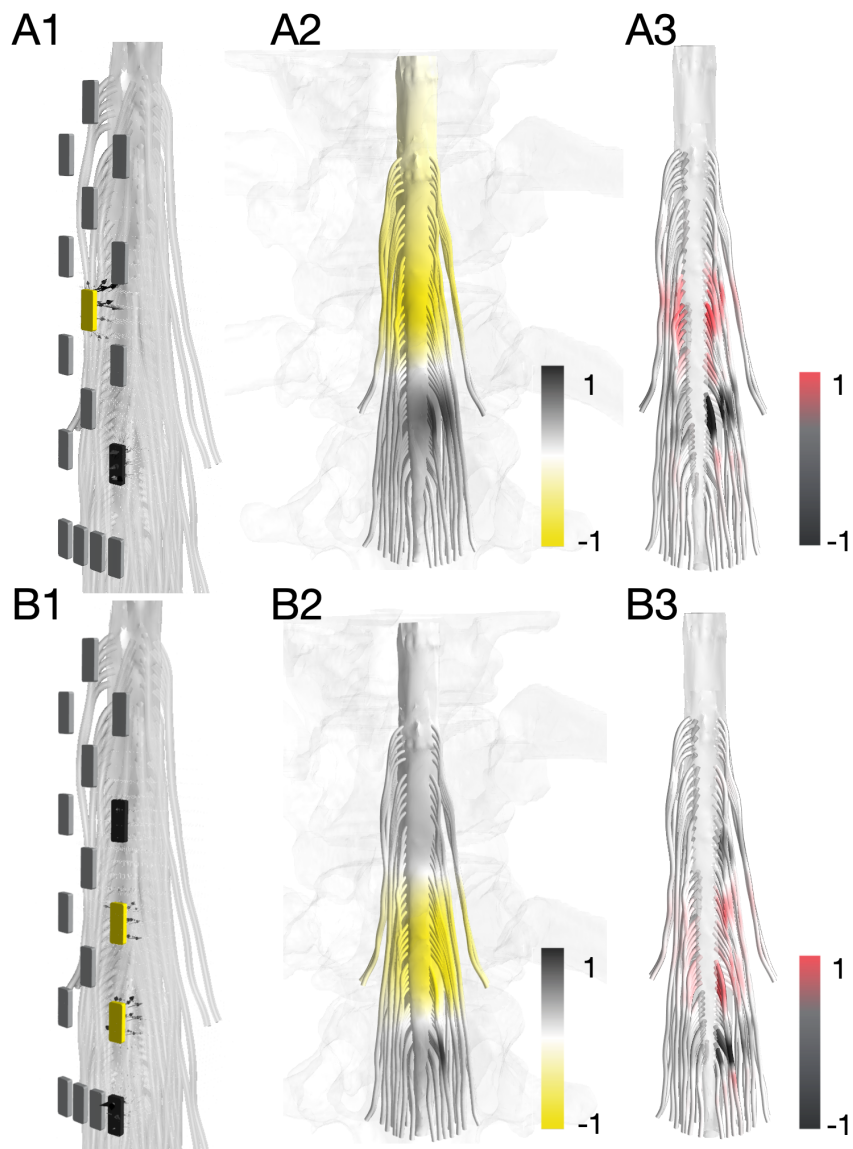


Figure 3.1: Multipolar simulations. The outcomes of both single cathode (highlighted in yellow) and single anode (highlighted in black) configurations, noted as A, as well as cases involving multiple cathodes and anodes, noted as B. The current flows from cathodes to anodes. Here, A1 and B1 show the different placement of cathodes and anodes and the current flow. A2 and B2 show the voltage distribution from the EM field. A3 and B3 show the AF value distribution over the spinal roots.

configurations: one monopolar configuration, i.e. a single cathode and a single anode, and one multipolar configuration, i.e. several cathodes and anodes.

On the left panels of Figure 3.1, we show the chosen electrode configuration as well as the flow of current. As we can see, the current flows from the cathodes to the anodes. In the middle panels, the color represents the relative magnitude of the potential distribution along the spinal cord. Finally, the right panels give access to the AF value along the spinal roots. Therefore, the visualization tool offers a preliminary estimate of the activated roots. The concrete calculation requires the nerve fibers' threshold values, which would be obtained from the optimization of the ANN. It is worth saying that the scale is normalized between  $-1$  and  $1$  since the equation is linear and only the relative value, matters in the visualization.

The electrical distribution in sub-figure A is not symmetric due to the fact that the spinal cord is not symmetric in reality and the placement of the electrode is neither in the precise middle. The precision of our model can not be calculated since no measurement has been performed inside the patient's body. As we argued in Section 2.6, the only to validate our model is to see if we manage to have a relatively small error in predicting the muscle activation.

In general, one can trust the visualization is able to give a close estimation of the electrical distribution over the spinal cord. Because the model is generated from the CT/MRI scan and the commercial software Sim4life, which has been approved for medical usage. Then, the error can only generated regarding our simplification pick of the tissues and the precision of the scan and the algorithm to build up the model, which are considerably acceptable as we have argued before.

## 3.2 Optimization of the Current Configuration for Root Activation

Activating different roots can lead to the activation of different muscle groups, which could cause different movement patterns. Thus, we would like to enable the EES to activate roots selectively. Here, having the current-basis of solution representing EES stimulations, we can now obtain the root activation level for any electrode configuration, and it is calculated from Equation 2.14. Using the algorithm presented in [31], we can optimize the root activation to reach a desired pattern. The algorithm is exactly the same as in [31], except that it outputs the values of the electrode in current and not in voltage.

To illustrate how the optimizer works, we give two examples in Figure

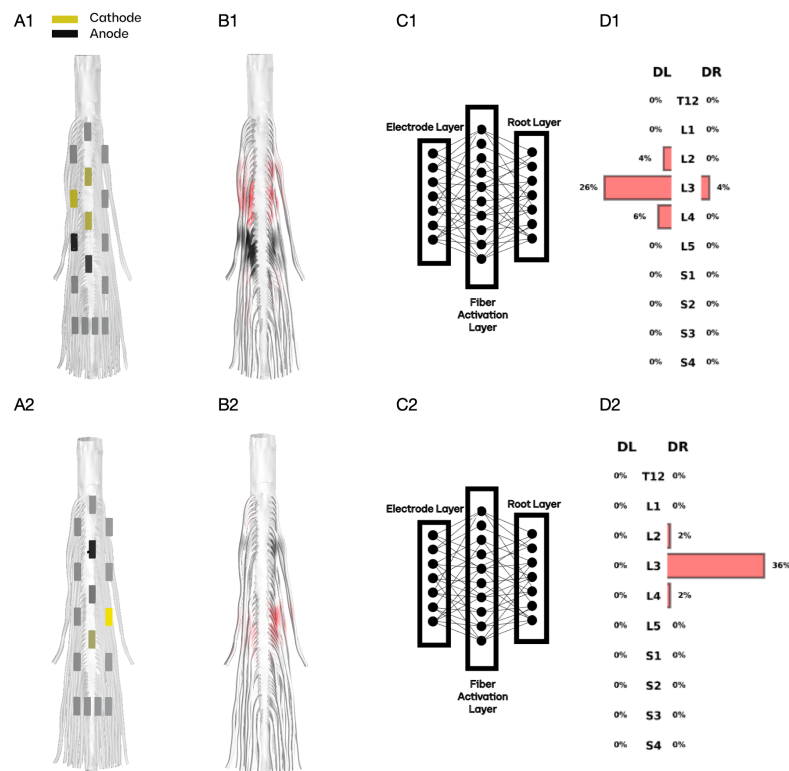


Figure 3.2: The resulting root activation from optimization. A1: The position of the cathodes and anodes is shown. The value over cathodes is  $-0.1\text{mA}$  and the anode on the left is  $0.1\text{mA}$  while the other one is  $0.2\text{mA}$ . B1: Visualization of the Activation Function values alongside the spinal cord. D1: Activated percentage of each root, obtained by the optimizer. The goal is to activate the dorsal left L3  $40\%$ . Here,  $25\%$  activation of the L3 dorsal left spinal root is achieved, while not obviously activating the other roots. A2: Cathodes -  $0.04\text{mA}$ ,  $-0.01\text{mA}$ ; Anode  $0.04\text{mA}$ ,  $0.01\text{mA}$ . B2: Activation Function. D2: The goal is to activate the dorsal right L3  $40\%$ . Here,  $36\%$  activation of it is achieved. C1 and C2 illustrate the network structure to generate the root activation.

**3.2.** Assuming the desired - target - root activation to be  $40\%$  activation at L3 dorsal left or  $40\%$  activation at L3 dorsal left, with the optimization network, we obtained  $25\%$  activation of the L3 dorsal left spinal root and  $36\%$  activation of the L3 dorsal right spinal root.

The MSE loss for the L3 dorsal left case is shown in fig. 3.3. Once the loss is converging, we stop the algorithm and check for the electrode configurations. From the previous examples, we could conclude that the

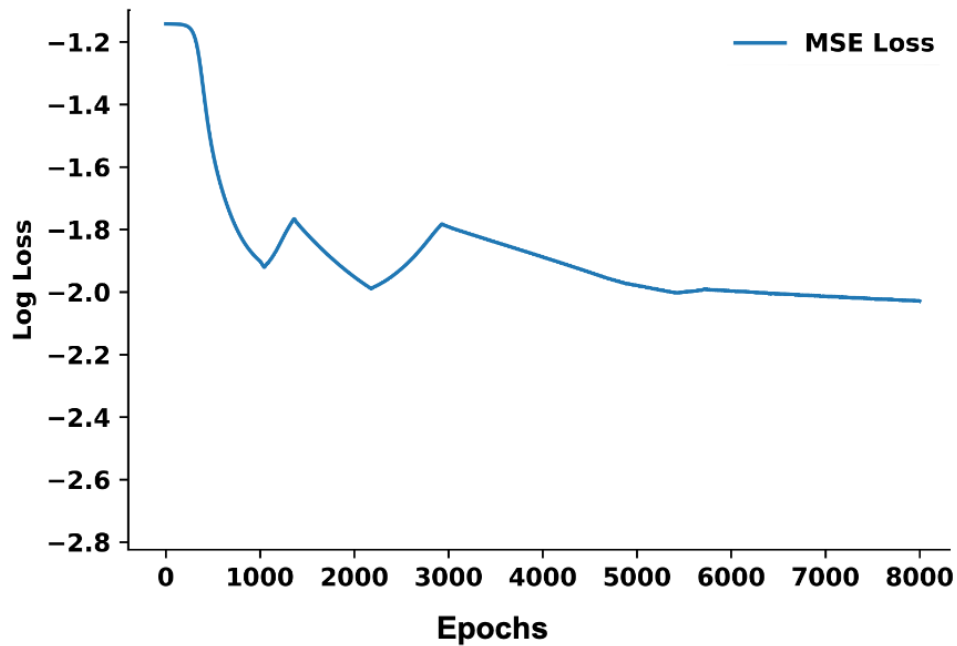


Figure 3.3: Loss curve of targeting 40% activation at L3 dorsal left root using the optimization algorithm provided in [31].

optimization algorithm provides a way of finding the optimal configurations with our FEM simulation results, given certain root targeting activation percentages.

### 3.3 Prediction of Muscle Activation

Predictive models are a valuable tool for neuroscientists. By providing insights into the spinal cord function, having an accurate predictive model of the spinal cord could help us to better understand the way EES works. By predicting the muscle activation given certain electrode configurations, if the model can perform generalization ability over the test dataset, we then have the chance to predict the effect of possible movement without having extra clinical trials.

With the methodology introduced in Section 2.5, we illustrate how our CyberSpine model - which combines both ANN and FEM - becomes a good predictor of EES-induced motor activation. We trained the framework using the STIMO dataset - the training was made using 80 percent of the data. Then, to acknowledge the prediction capability of our CyberSpine model, we tested

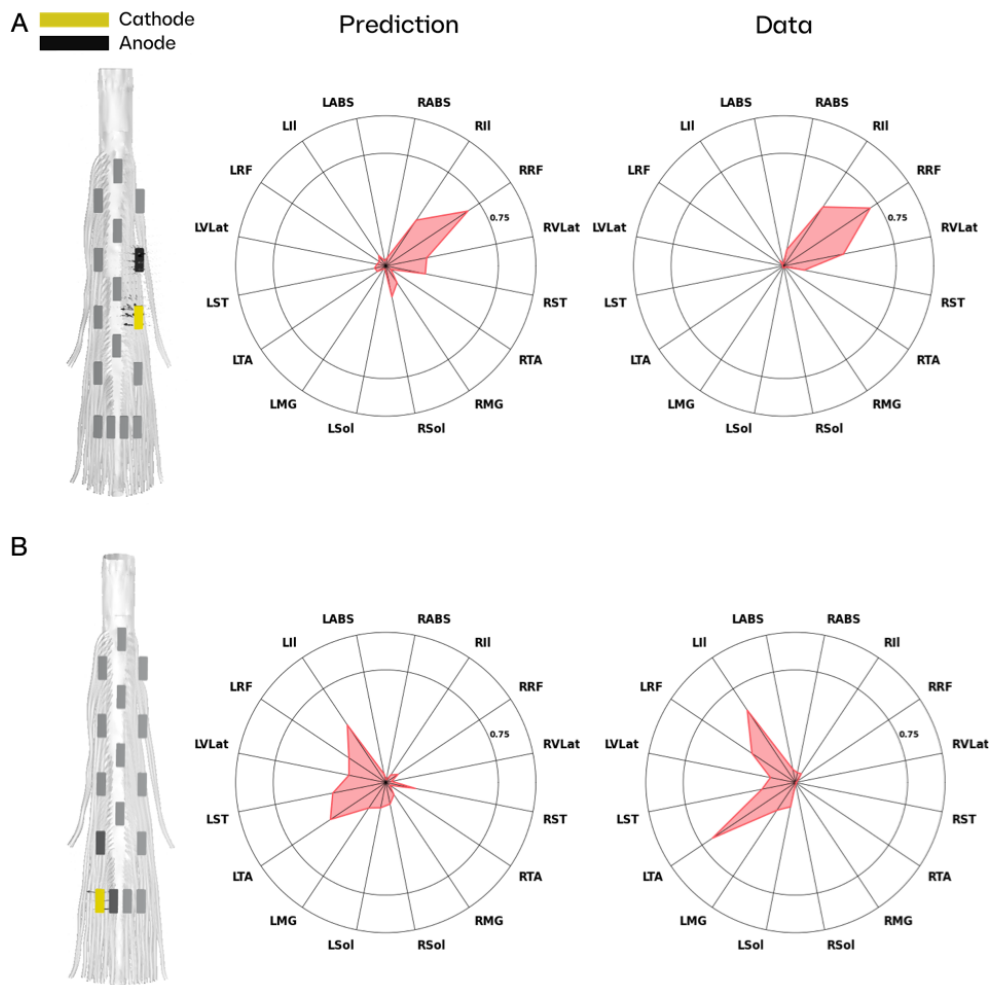


Figure 3.4: Two prediction examples of muscle activation. EMG Prediction with cathode and anode position shown on the left. The true data are shown on the right. A: Cathode  $-2.5\text{mA}$ ; Anode  $2.5\text{mA}$ . B: Cathode  $-4\text{mA}$ ; Anodes  $2\text{mA}$  for each. The prediction for Left(L)/Right(R) Abdominal(Abs), Iliacus(IL), Rectus Femoris (RF), Vastus Lateralis (VLat), Sartorius (ST), Tibialis Anterior (TA), Gastrocnemius Medialis (MG), and Soleus (Sol) are shown here.

the prediction against 20 percent of the remaining data, i.e. the part of the data not seen during training.

The cost function to minimize was defined as the deviation between the muscle activity generated by the CyberSpine model and the recorded muscle activity, see Section 2.5 for details. The fitting procedure took into account all

the electrode active sites and stimulation amplitude configurations currently available in the STIMO dataset.

The overall learning curve regarding the loss defined in 2.17 for the training dataset is shown in Figure 3.5.

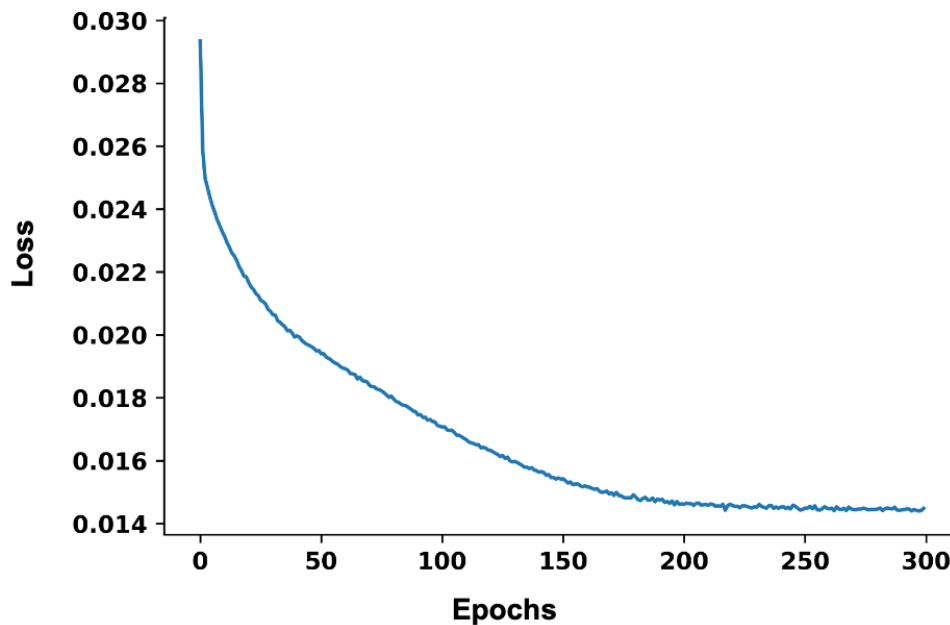


Figure 3.5: Loss curve of training the ANN to predict the muscle activation in the training dataset.

To illustrate how the predictive CyberSpine model works, we show two examples of muscle activation prediction in Figure 3.4. As we can see, the muscle activation predicted by our framework is very similar to the muscle pattern recorded in the patient.

To quantify the overall prediction capability, we computed the average error done by the CyberSpine. The absolute average error is presented in Figure 3.6 A and B. As we can see, the average error is very small — almost all below 15 percent — meaning that on average the predictions are rather satisfying.

The results overall show good generalization ability, which could lead to potential clinical usage to replace the time-consuming procedure of trying different configurations to activate certain muscles once you have the previously collected dataset. Both the training data and the testing data are from the same patient.

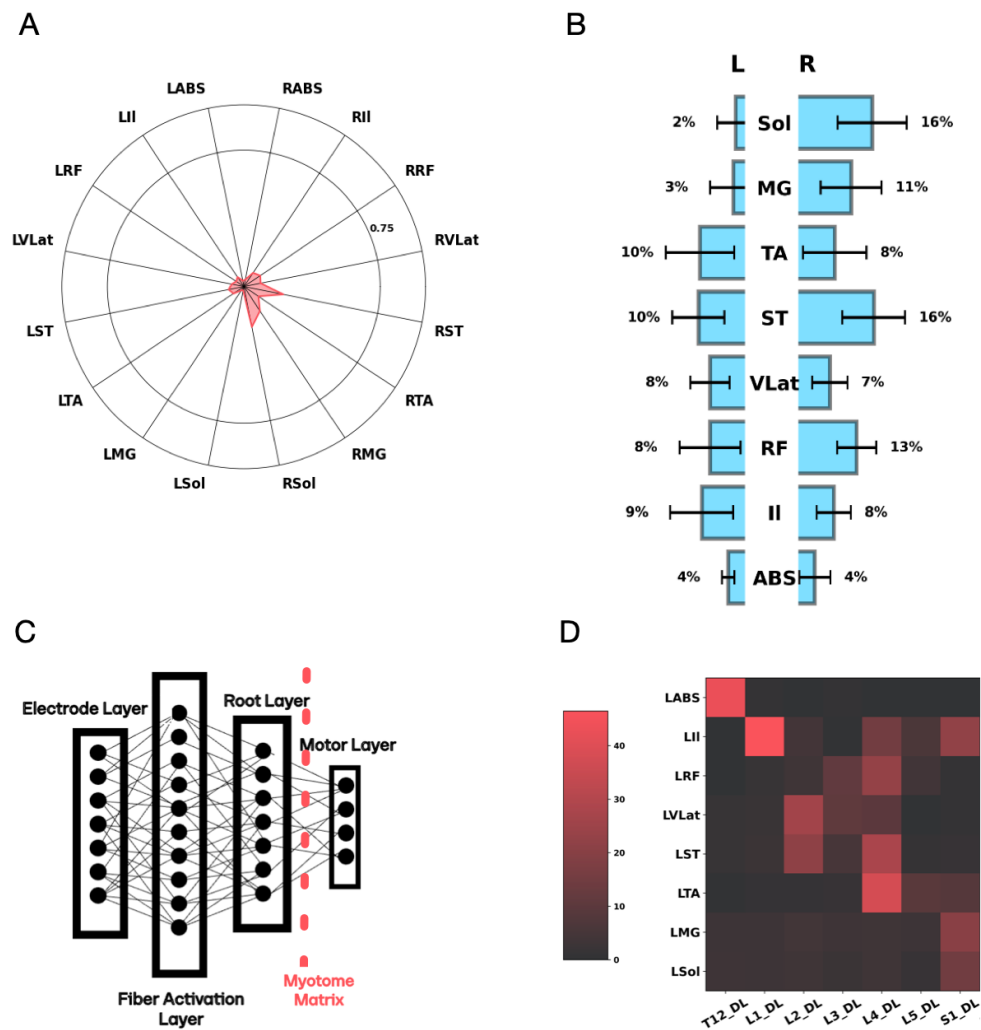


Figure 3.6: Absolute prediction error and the myotome matrix. A: Average absolute prediction error in radar plot. The prediction for Left(L)/Right(R) Abdominal(Abs), Iliacus(IL), Rectus Femoris (RF), Vastus Lateralis (VLat), Sartorius (ST), Tibialis Anterior (TA), Gastrocnemius Medialis (MG), and Soleus (Sol) are shown here. B: A more detailed bar plot of the prediction results. The average absolute prediction errors for each muscle activation are shown as the numbers. The line represents the variation of the prediction error within each muscle's dataset. C: Illustration of the position of myotome matrix  $J$  inside the Neural Network. D: Visualization of the myotome matrix. The matrix has the "diagonal" tendency.

### 3.4 Emergence of Myotome

Biological information extraction can help us improve our understanding of biological systems by identifying and extracting relevant information from datasets. This information can be used to identify new relationships between biological entities. In this section, we take advantage of our framework to extract the myotome, that is, the matrix of connection between the dorsal roots and muscles. Specifically, Myotome represents the linkage distribution from spinal roots to muscles.

To do so, we made use of recent techniques of artificial intelligence which provide new approaches for neuroscientists to uncover circuit connectivity.

This framework has been successfully used to answer a wide range of neuroscientific questions, for instance, it has been employed to model different aspects of sensory, cognitive, and motor circuits. Specifically, we trained the CyberSpine model to predict motor activation while constraining the network to keep track of the anatomy of the spinal cord.

As described in Section 2.5, alongside the convergence of our network, it provides certain interpretability. By directly training the spine network model on stimulus-induced muscle response, the CyberSpine model provides a way to efficiently generate a personalized myotome matrix that otherwise could be near impossible to extract. Indeed, once the ANN has converged, the  $J$  matrix after optimization is obtained and shown in Figure 3.6.

As one can see, the result is coherent with the "diagonal" tendency discussed in Section 2.6. This kind of "diagonal" tendency again proves that our network is kind of explainable. From the previous papers, it is hard to conclude if there exists a common agreement on how the myotome matrix should exactly look like since it varies between individuals, then it is hard to evaluate our result.

There exists one result in [9] on the same patient we have. Compared to their results, we obtained almost the same structure, except the Left Iliacus(LII) links to the S1 dorsal left (S1\_DL). However, we do observe the activation of the Left Iliacus when stimulating the S1 dorsal left during the clinical trial, which is coherent with our result. We guess it is caused by the feedback from the reflex arc, which requires further experiments. In general, this "diagonal" tendency follows the anatomical structure of the human body. Thus, we have reason to believe that this matrix reflects the real linkage situation from roots to muscles within the patient, who we collect the data from.



## Chapter 4

# Conclusions and Future work

### 4.1 Conclusions

Over the past few years, computational models have become a powerful tool in analyzing the immediate effects of EES. Most phenomena reported during EES, such as nerve fiber recruitment and muscle responses, for instance, are well reproduced by the model. Moreover, it has become a useful tool in the optimization of electrode design and it has played an important part in guiding decision-making for the electrode placement during surgery. However, the model remains a simplification of the actual patient's spine and improvements are still needed to cover all salient features of empirical data. A personalized spine model taking into account the nonlinear dynamics of spinal circuits is still lacking.

Due to the limited knowledge of the connectivity diagrams of spinal circuits, biologically constrained artificial intelligence appears to be the cleverest alternative. In this master thesis, we used this approach to study EES-induced motor response. To do so, we have implemented a multipolar basis of solution of the Poisson equation, coupled the basis to an artificial neural network, and trained the ANN layers against the patient's actual data. We have shown that the resulting CyberSpine model was able to predict accurately EES-induced motor response. Furthermore, we illustrated how our model became handy in extracting biologically relevant information regarding the efficient connectivity of the patient's spine. Therefore the goals set in Section 1.5 have been accomplished.

## 4.2 Limitations

In the thesis, we implemented an Artificial Neural Network (ANN) to mimic the neural link between the spinal roots and motor neurons. Usually, such a strategy requires a large dataset for training. However, only 669 trials of data were available for our project. More data might be required to minimize prediction errors and increase the statistical significance of the myotome matrix. Furthermore, to get more reliable results, the real validation would consist of testing the CyberSpine model during a new session with the patient.

## 4.3 Future work

Testing our prediction results during new clinical sessions would be the first step as it would offer a true validation and ensure the effectiveness of the CyberSpine model.

Secondly, within this thesis, we have implemented the quasi-static simulation, which caused the absence of the time domain information. We pre-processed the EMG data into the maximum activated percentage for the same reason. Thus, in the future, it would be relevant to study how the myotome changes for different choices of stimulation frequency, as it has been observed that different muscles are activated under different stimulation frequencies. With more time domain information, training against kinematic instead of muscle activation would also be a possibility. Directly predicting the kinematics is even more useful, because restoring walking is the final goal, and knowing the motor activation is only an intermediate link.

Besides restoring walking, it would be also interesting to transfer our results to the upper limb movement. Since the upper limb has a greater degree of freedom than the lower limb, it would be useful for finding the proper stimulation configurations during EES.

## 4.4 Reflections

The overall work is very interesting and was carried out as scheduled. However, unnecessary time was wasted when doing the simulations due to the details of the math were not fully understood before starting the simulations. For future projects, a full understanding of the methodology is a must before starting the experiment to avoid blind debugging time.

## **4.5 Ethics**

The data and all clinical test is collected as part of the clinically feasible study STIMO. This study was approved by the Swiss ethical authorities (Swissethics protocol number 04/2014 project ID PB\_2016-00886, Swissmedic protocol 2016-MD-0002) and was conducted in accordance with the Declaration of Helsinki. All participants signed a written informed consent before their participation. More information at [www.clinicaltrials.gov](http://www.clinicaltrials.gov) (NCT02936453). All surgical and experimental procedures were performed at the Lausanne University Hospital (CHUV).

## **4.6 Sustainability**

The thesis provides a possible solution for gaining a better understanding of treating spinal cord injury patients. It supports human health and provides a sustainable solution for society since the only consumption after implantation of the EES electrodes is electricity, which can potentially be generated by solar energy.



# List of Figures

|     |   |   |
|-----|---|---|
| 1.1 | EES rehabilitation equipment. EES electrodes together with the body weight support equipment form one type of rehabilitation system aiming to help the patients walk. (Figure adapted from [17]) . . . . .                        | 2 |
| 1.2 | Ideal muscle activation through EES for key phases of gait. Electrodes alongside give examples of EES configurations for one specific patient to activate the corresponding muscle groups. (Figure adapted from [9]) . . . . .    | 2 |
| 1.3 | Typical EES clinical timeline. The whole procedure contains inclusion, surgery, EES configuration, rehabilitation with EES, and use of EES during study extension. (Figure adapted from [9]) . . . . .                            | 2 |
| 1.4 | CNS anatomy. The spinal cord includes the cervical, thoracic, lumbar, and sacral segments. (Figure adapted from [18]) . . . .   | 4 |
| 1.5 | Anatomical structure of the spinal cord. (Figure adapted from [19]) . . . . .   | 5 |
| 1.6 | Division of the vertebrae along the spinal column, including cervical (C), thoracic (T), lumbar (L), and sacral (S) segments. (Figure adapted from [1]) . . . . .   | 6 |
| 1.7 | 3D personalized structural model built from CT scan MRI images. (Figure adapted from [9]) . . . . .   | 7 |
| 1.8 | EES electrode placement and the relative position with the Spinal Segments with cathodes in yellow and anodes in black. In the figure, one configuration is shown and the activation of the roots should be around L3-L5. . . . . | 8 |

|     |  |    |
|-----|--|----|
| 2.1 | Workflow of the project. The Finite Element Model (FEM) takes the anatomical model and the tissue conductivity as given. Then, after performing Electroquasistatic Electro-magnetic Simulation, the basis of the solutions to performed multipolar simulations is stored and used as input of the ANN. Taking any electrode configurations, the ANN calculates the Activation Function and trains to output EMG data. . . . .  | 14 |
| 2.2 | An example of one trial of EMG data. The EES is set to 20Hz and 3.5mA, with electrodes No.4 as the cathode and electrodes No.3 and 5 as anodes. The left and right refer to the left and right lower limbs. The figure is plotted within the time domain. The red line represents the pulses of EES. Iliacus(IL), Rectus Femoris (RF), Vastus Lateralis (Vlat), Sartorius (ST), Tibialis Anterior (TA), Gastrocnemius Medialis (MG), and Soleus (Sol) EMG signals are shown here. . . . .            | 15 |
| 2.3 | Anatomical model and its associated Finite Element model. A: Outlook of the anatomical model. The model includes bones, discs, white matter, spinal roots, and EES paddles. B: The figure displays the resulting finite element model obtained after the voxelisation of the anatomical model. . . . .   | 18 |
| 3.1 | Multipolar simulations. The outcomes of both single cathode (highlighted in yellow) and single anode (highlighted in black) configurations, noted as A, as well as cases involving multiple cathodes and anodes, noted as B. The current flows from cathodes to anodes. Here, A1 and B1 show the different placement of cathodes and anodes and the current flow. A2 and B2 show the voltage distribution from the EM field. A3 and B3 show the AF value distribution over the spinal roots. . . . . | 28 |

|     |   |    |
|-----|---|----|
| 3.2 | The resulting root activation from optimization. A1: The position of the cathodes and anodes is shown. The value over cathodes is -0.1mA and the anode on the left is 0.1mA while the other one is 0.2mA. B1: Visualization of the Activation Function values alongside the spinal cord. D1: Activated percentage of each root, obtained by the optimizer. The goal is to activate the dorsal left L3 40%. Here, 25% activation of the L3 dorsal left spinal root is achieved, while not obviously activating the other roots. A2: Cathodes -0.04mA, -0.01mA; Anode 0.04mA, 0.01mA. B2: Activation Function. D2: The goal is to activate the dorsal right L3 40%. Here, 36% activation of it is achieved. C1 and C2 illustrate the network structure to generate the root activation. . . . . | 30 |
| 3.3 | Loss curve of targeting 40% activation at L3 dorsal left root using the optimization algorithm provided in [31]. . . . .  | 31 |
| 3.4 | Two prediction examples of muscle activation. EMG Prediction with cathode and anode position shown on the left. The true data are shown on the right. A: Cathode -2.5mA; Anode 2.5mA. B: Cathode -4mA; Anodes 2mA for each. The prediction for Left(L)/Right(R) Abdominal(Abs), Iliacus(IL), Rectus Femoris (RF), Vastus Lateralis (VLat), Sartorius (ST), Tibialis Anterior (TA), Gastrocnemius Medialis (MG), and Soleus (Sol) are shown here. . . . .  | 32 |
| 3.5 | Loss curve of training the ANN to predict the muscle activation in the training dataset. . . . .  | 33 |
| 3.6 | Absolute prediction error and the myotome matrix. A: Average absolute prediction error in radar plot. The prediction for Left(L)/Right(R) Abdominal(Abs), Iliacus(IL), Rectus Femoris (RF), Vastus Lateralis (VLat), Sartorius (ST), Tibialis Anterior (TA), Gastrocnemius Medialis (MG), and Soleus (Sol) are shown here. B: A more detailed bar plot of the prediction results. The average absolute prediction errors for each muscle activation are shown as the numbers. The line represents the variation of the prediction error within each muscle's dataset. C: Illustration of the position of myotome matrix $J$ inside the Neural Network. D: Visualization of the myotome matrix. The matrix has the "diagonal" tendency. . .  | 34 |



# List of Tables

2.1 Conductivity Parameters . . . . . 17



## List of acronyms and abbreviations

|     |                                 |
|-----|---------------------------------|
| AF  | Activation Function             |
| ANN | Artificial Neural Network       |
| CNS | Central Nervous System          |
| EES | Epidural Electrical Stimulation |
| EM  | Electromagnetism                |
| EMG | Electromyography                |
| FEM | Finite Element Model            |
| ICC | Integrated Current Condition    |
| OT  | Optimal Transport               |
| SCI | Spinal Cord Injury              |



# References

- [1] J. Bickenbach, A. Officer, T. Shakespeare, P. von Groote, World Health Organization, and The International Spinal Cord Society, *International perspectives on spinal cord injury / edited by Jerome Bickenbach ... [et al]*. Geneva: World Health Organization, 2013. ISBN 978-92-4-156466-3 Section: xiii, 231 p. [Online]. Available: <https://apps.who.int/iris/handle/10665/94190> [Pages 1, 6, and 41.]
- [2] C. Kathe, M. A. Skinnider, T. H. Hutson, N. Regazzi, M. Gautier, R. Demesmaeker, S. Komi, S. Ceto, N. D. James, N. Cho, L. Baud, K. Galan, K. J. E. Matson, A. Rowald, K. Kim, R. Wang, K. Minassian, J. O. Prior, L. Asboth, Q. Barraud, S. P. Lacour, A. J. Levine, F. Wagner, J. Bloch, J. W. Squair, and G. Courtine, “The neurons that restore walking after paralysis,” *Nature*, vol. 611, no. 7936, pp. 540–547, Nov. 2022. doi: 10.1038/s41586-022-05385-7. [Online]. Available: <https://www.nature.com/articles/s41586-022-05385-7> [Page 1.]
- [3] R. M. Ichiyama, G. Courtine, Y. P. Gerasimenko, G. J. Yang, R. Van Den Brand, I. A. Lavrov, H. Zhong, R. R. Roy, and V. R. Edgerton, “Step Training Reinforces Specific Spinal Locomotor Circuitry in Adult Spinal Rats,” *The Journal of Neuroscience*, vol. 28, no. 29, pp. 7370–7375, Jul. 2008. doi: 10.1523/JNEUROSCI.1881-08.2008. [Online]. Available: <https://www.jneurosci.org/lookup/doi/10.1523/JNEUROSCI.1881-08.2008> [Page 1.]
- [4] G. Courtine, Y. Gerasimenko, R. Van Den Brand, A. Yew, P. Musienko, H. Zhong, B. Song, Y. Ao, R. M. Ichiyama, I. Lavrov, R. R. Roy, M. V. Sofroniew, and V. R. Edgerton, “Transformation of nonfunctional spinal circuits into functional states after the loss of brain input,” *Nature Neuroscience*, vol. 12, no. 10, pp. 1333–1342, Oct. 2009. doi: 10.1038/nn.2401. [Online]. Available: <https://www.nature.com/articles/nn.2401> [Page 1.]

- [5] N. Wenger, E. M. Moraud, S. Raspopovic, M. Bonizzato, J. DiGiovanna, P. Musienko, M. Morari, S. Micera, and G. Courtine, “Closed-loop neuromodulation of spinal sensorimotor circuits controls refined locomotion after complete spinal cord injury,” *Science Translational Medicine*, vol. 6, no. 255, Sep. 2014. doi: 10.1126/scitranslmed.3008325. [Online]. Available: <https://www.science.org/doi/10.1126/scitranslmed.3008325> [Page 1.]
- [6] N. Wenger, E. M. Moraud, J. Gandar, P. Musienko, M. Capogrosso, L. Baud, C. G. Le Goff, Q. Barraud, N. Pavlova, N. Dominici, I. R. Minev, L. Asboth, A. Hirsch, S. Duis, J. Kreider, A. Mortera, O. Haverbeck, S. Kraus, F. Schmitz, J. DiGiovanna, R. Van Den Brand, J. Bloch, P. Detemple, S. P. Lacour, E. Bézard, S. Micera, and G. Courtine, “Spatiotemporal neuromodulation therapies engaging muscle synergies improve motor control after spinal cord injury,” *Nature Medicine*, vol. 22, no. 2, pp. 138–145, Feb. 2016. doi: 10.1038/nm.4025. [Online]. Available: <https://www.nature.com/articles/nm.4025> [Page 1.]
- [7] L. Asboth, L. Friedli, J. Beauparlant, C. Martinez-Gonzalez, S. Anil, E. Rey, L. Baud, G. Pidpruzhnykova, M. A. Anderson, P. Shkorbatova, L. Batti, S. Pagès, J. Kreider, B. L. Schneider, Q. Barraud, and G. Courtine, “Cortico–reticulo–spinal circuit reorganization enables functional recovery after severe spinal cord contusion,” *Nature Neuroscience*, vol. 21, no. 4, pp. 576–588, Apr. 2018. doi: 10.1038/s41593-018-0093-5. [Online]. Available: <https://www.nature.com/articles/s41593-018-0093-5> [Page 1.]
- [8] M. Capogrosso, T. Milekovic, D. Borton, F. Wagner, E. M. Moraud, J.-B. Mignardot, N. Buse, J. Gandar, Q. Barraud, D. Xing, E. Rey, S. Duis, Y. Jianzhong, W. K. D. Ko, Q. Li, P. Detemple, T. Denison, S. Micera, E. Bezard, J. Bloch, and G. Courtine, “A brain–spine interface alleviating gait deficits after spinal cord injury in primates,” *Nature*, vol. 539, no. 7628, pp. 284–288, Nov. 2016. doi: 10.1038/nature20118. [Online]. Available: <https://www.nature.com/articles/nature20118> [Page 1.]
- [9] A. Rowald, S. Komi, R. Demesmaeker, E. Baaklini, S. D. Hernandez-Charpak, E. Paoles, H. Montanaro, A. Cassara, F. Becce, B. Lloyd, T. Newton, J. Ravier, N. Kinany, M. D’Ercole, A. Paley, N. Hankov, C. Varescon, L. McCracken, M. Vat, M. Caban, A. Watrin, C. Jacquet, L. Bole-Feysot, C. Harte, H. Lorach, A. Galvez, M. Tschopp,

- N. Herrmann, M. Wacker, L. Geernaert, I. Fodor, V. Radevich, K. Van Den Keybus, G. Eberle, E. Pralong, M. Roulet, J.-B. Ledoux, E. Fornari, S. Mandija, L. Mattera, R. Martuzzi, B. Nazarian, S. Benkler, S. Callegari, N. Greiner, B. Fuhrer, M. Froeling, N. Buse, T. Denison, R. Buschman, C. Wende, D. Ganty, J. Bakker, V. Delattre, H. Lambert, K. Minassian, C. A. T. Van Den Berg, A. Kavounoudias, S. Micera, D. Van De Ville, Q. Barraud, E. Kurt, N. Kuster, E. Neufeld, M. Capogrosso, L. Asboth, F. B. Wagner, J. Bloch, and G. Courtine, “Activity-dependent spinal cord neuromodulation rapidly restores trunk and leg motor functions after complete paralysis,” *Nature Medicine*, vol. 28, no. 2, pp. 260–271, Feb. 2022. doi: 10.1038/s41591-021-01663-5. [Online]. Available: <https://www.nature.com/articles/s41591-021-01663-5> [Pages 1, 2, 7, 9, 10, 24, 35, and 41.]
- [10] S. Harkema, Y. Gerasimenko, J. Hodes, J. Burdick, C. Angeli, Y. Chen, C. Ferreira, A. Willhite, E. Rejc, R. G. Grossman, and V. R. Edgerton, “Effect of epidural stimulation of the lumbosacral spinal cord on voluntary movement, standing, and assisted stepping after motor complete paraplegia: a case study,” *The Lancet*, vol. 377, no. 9781, pp. 1938–1947, Jun. 2011. doi: 10.1016/S0140-6736(11)60547-3. [Online]. Available: <https://linkinghub.elsevier.com/retrieve/pii/S0140673611605473> [Page 1.]
- [11] E. Formento, K. Minassian, F. Wagner, J. B. Mignardot, C. G. Le Goff-Mignardot, A. Rowald, J. Bloch, S. Micera, M. Capogrosso, and G. Courtine, “Electrical spinal cord stimulation must preserve proprioception to enable locomotion in humans with spinal cord injury,” *Nature Neuroscience*, vol. 21, no. 12, pp. 1728–1741, Dec. 2018. doi: 10.1038/s41593-018-0262-6. [Online]. Available: <https://www.nature.com/articles/s41593-018-0262-6> [Pages 1 and 3.]
- [12] S. M. Danner, U. S. Hofstoetter, B. Freundl, H. Binder, W. Mayr, F. Rattay, and K. Minassian, “Human spinal locomotor control is based on flexibly organized burst generators,” *Brain*, vol. 138, no. 3, pp. 577–588, Mar. 2015. doi: 10.1093/brain/awu372. [Online]. Available: <https://academic.oup.com/brain/article-lookup/doi/10.1093/brain/awu372> [Page 1.]
- [13] M. L. Gill, P. J. Grahn, J. S. Calvert, M. B. Linde, I. A. Lavrov, J. A. Strommen, L. A. Beck, D. G. Sayenko, M. G. Van Straaten, D. I. Drubach, D. D. Veith, A. R. Thoreson, C. Lopez, Y. P. Gerasimenko,

- V. R. Edgerton, K. H. Lee, and K. D. Zhao, “Neuromodulation of lumbosacral spinal networks enables independent stepping after complete paraplegia,” *Nature Medicine*, vol. 24, no. 11, pp. 1677–1682, Nov. 2018. doi: 10.1038/s41591-018-0175-7. [Online]. Available: <https://www.nature.com/articles/s41591-018-0175-7> [Page 1.]
- [14] C. A. Angeli, M. Boakye, R. A. Morton, J. Vogt, K. Benton, Y. Chen, C. K. Ferreira, and S. J. Harkema, “Recovery of Over-Ground Walking after Chronic Motor Complete Spinal Cord Injury,” *New England Journal of Medicine*, vol. 379, no. 13, pp. 1244–1250, Sep. 2018. doi: 10.1056/NEJMoa1803588. [Online]. Available: <http://www.nejm.org/doi/10.1056/NEJMoa1803588> [Page 1.]
- [15] F. B. Wagner, J.-B. Mignardot, C. G. Le Goff-Mignardot, R. Demesmaeker, S. Komi, M. Capogrosso, A. Rowald, I. Seáñez, M. Caban, E. Pirondini, M. Vat, L. A. McCracken, R. Heimgartner, I. Fodor, A. Watrin, P. Seguin, E. Paoles, K. Van Den Keybus, G. Eberle, B. Schurch, E. Pralong, F. Becce, J. Prior, N. Buse, R. Buschman, E. Neufeld, N. Kuster, S. Carda, J. Von Zitzewitz, V. Delattre, T. Denison, H. Lambert, K. Minassian, J. Bloch, and G. Courtine, “Targeted neurotechnology restores walking in humans with spinal cord injury,” *Nature*, vol. 563, no. 7729, pp. 65–71, Nov. 2018. doi: 10.1038/s41586-018-0649-2. [Online]. Available: <https://www.nature.com/articles/s41586-018-0649-2> [Page 1.]
- [16] H. Lorach, A. Galvez, V. Spagnolo, F. Martel, S. Karakas, N. Interling, M. Vat, O. Faivre, C. Harte, S. Komi, J. Ravier, T. Collin, L. Coquoz, I. Sakr, E. Baaklini, S. D. Hernandez-Charpak, G. Dumont, R. Buschman, N. Buse, T. Denison, I. Van Nes, L. Asboth, A. Watrin, L. Struber, F. Sauter-Starace, L. Langar, V. Auboiroux, S. Carda, S. Chabardes, T. Aksenova, R. Demesmaeker, G. Charvet, J. Bloch, and G. Courtine, “Walking naturally after spinal cord injury using a brain–spine interface,” *Nature*, May 2023. doi: 10.1038/s41586-023-06094-5. [Online]. Available: <https://www.nature.com/articles/s41586-023-06094-5> [Page 1.]
- [17] <https://www.independent.ie/irish-news/health/scientists-hail-breakthrough-in-restoring-motor-function-after-paralysis-caused-by-spinal-injury/42132611.html>. [Pages 2 and 41.]

- [18] E. R. Kandel, Ed., *Principles of neural science*, 5th ed. New York: McGraw-Hill, 2013. ISBN 978-0-07-139011-8 [Pages 3, 4, and 41.]
- [19] O. Bican, A. Minagar, and A. A. Pruit, “The Spinal Cord,” *Neurologic Clinics*, vol. 31, no. 1, pp. 1–18, Feb. 2013. doi: 10.1016/j.ncl.2012.09.009. [Online]. Available: <https://linkinghub.elsevier.com/retrieve/pii/S0733861912000709> [Pages 5, 7, and 41.]
- [20] D. E. Rumelhart, G. E. Hinton, and R. J. Williams, “Learning representations by back-propagating errors,” *Nature*, vol. 323, no. 6088, pp. 533–536, Oct. 1986. doi: 10.1038/323533a0. [Online]. Available: <https://www.nature.com/articles/323533a0> [Pages 8 and 10.]
- [21] G. Cybenko, “Approximation by superpositions of a sigmoidal function,” *Mathematics of Control, Signals, and Systems*, vol. 2, no. 4, pp. 303–314, Dec. 1989. doi: 10.1007/BF02551274. [Online]. Available: <http://link.springer.com/10.1007/BF02551274> [Pages 8 and 9.]
- [22] B. A. Richards, T. P. Lillicrap, P. Beaudoin, Y. Bengio, R. Bogacz, A. Christensen, C. Clopath, R. P. Costa, A. De Berker, S. Ganguli, C. J. Gillon, D. Hafner, A. Kepecs, N. Kriegeskorte, P. Latham, G. W. Lindsay, K. D. Miller, R. Naud, C. C. Pack, P. Poirazi, P. Roelfsema, J. Sacramento, A. Saxe, B. Scellier, A. C. Schapiro, W. Senn, G. Wayne, D. Yamins, F. Zenke, J. Zylberberg, D. Therien, and K. P. Kording, “A deep learning framework for neuroscience,” *Nature Neuroscience*, vol. 22, no. 11, pp. 1761–1770, Nov. 2019. doi: 10.1038/s41593-019-0520-2. [Online]. Available: <https://www.nature.com/articles/s41593-019-0520-2> [Pages 8, 10, and 11.]
- [23] A. Saxe, S. Nelli, and C. Summerfield, “If deep learning is the answer, what is the question?” *Nature Reviews Neuroscience*, vol. 22, no. 1, pp. 55–67, Jan. 2021. doi: 10.1038/s41583-020-00395-8. [Online]. Available: <https://www.nature.com/articles/s41583-020-00395-8> [Page 8.]
- [24] S. Schneider, J. H. Lee, and M. W. Mathis, “Learnable latent embeddings for joint behavioural and neural analysis,” *Nature*, vol. 617, no. 7960, pp. 360–368, May 2023. doi: 10.1038/s41586-023-06031-6. [Online]. Available: <https://www.nature.com/articles/s41586-023-06031-6> [Page 8.]

- [25] N. A. Greiner, “Refinements of hybrid neurophysical volume conductor models and application to study epidural electrical stimulation of the cervical spinal cord,” Mar. 2020. doi: 10.5075/EPFL-THESIS-7970 Publisher: Lausanne, EPFL. [Online]. Available: <http://infoscience.epfl.ch/record/276224> [Pages 9, 10, 16, and 19.]
- [26] F. Rattay, K. Minassian, and M. Dimitrijevic, “Epidural electrical stimulation of posterior structures of the human lumbosacral cord: 2. quantitative analysis by computer modeling,” *Spinal Cord*, vol. 38, no. 8, pp. 473–489, Aug. 2000. doi: 10.1038/sj.sc.3101039. [Online]. Available: <https://www.nature.com/articles/3101039> [Page 9.]
- [27] M. Capogrosso, N. Wenger, S. Raspopovic, P. Musienko, J. Beauparlant, L. Bassi Luciani, G. Courtine, and S. Micera, “A Computational Model for Epidural Electrical Stimulation of Spinal Sensorimotor Circuits,” *The Journal of Neuroscience*, vol. 33, no. 49, pp. 19 326–19 340, Dec. 2013. doi: 10.1523/JNEUROSCI.1688-13.2013. [Online]. Available: <https://www.jneurosci.org/lookup/doi/10.1523/JNEUROSCI.1688-13.2013> [Pages 9 and 17.]
- [28] J. Meier, W. Rotten, A. Zoutman, H. Boom, and P. Bergveld, “Simulation of multipolar fiber selective neural stimulation using intrafascicular electrodes,” *IEEE Transactions on Biomedical Engineering*, vol. 39, no. 2, pp. 122–134, Feb. 1992. doi: 10.1109/10.121643. [Online]. Available: <http://ieeexplore.ieee.org/document/121643/> [Page 9.]
- [29] L. N. Govindarajan, J. S. Calvert, S. R. Parker, M. Jung, R. Darie, P. Miranda, E. Shaaya, D. A. Borton, and T. Serre, “Fast inference of spinal neuromodulation for motor control using amortized neural networks,” *Journal of Neural Engineering*, vol. 19, no. 5, p. 056037, Oct. 2022. doi: 10.1088/1741-2552/ac9646. [Online]. Available: <https://iopscience.iop.org/article/10.1088/1741-2552/ac9646> [Pages 9 and 10.]
- [30] L. Liang, A. Damiani, M. Del Brocco, E. R. Rogers, M. K. Jantz, L. E. Fisher, R. A. Gaunt, M. Capogrosso, S. F. Lempka, and E. Pirondini, “A systematic review of computational models for the design of spinal cord stimulation therapies: from neural circuits to patient-specific simulations,” *The Journal of Physiology*, vol. 601, no. 15, pp. 3103–3121, Aug. 2023. doi: 10.1113/JP282884. [Online]. Available: <https://physoc.onlinelibrary.wiley.com/doi/10.1113/JP282884> [Page 9.]

- [31] J. G. Ordonez, “In-silico optimization of spinal electrical stimulation,” 2022. [Pages 9, 10, 21, 23, 29, 31, and 43.]
- [32] J. P. Reilly, V. T. Freeman, and W. D. Larkin, “Sensory Effects of Transient Electrical Stimulation - Evaluation with a Neuroelectric Model,” *IEEE Transactions on Biomedical Engineering*, vol. BME-32, no. 12, pp. 1001–1011, Dec. 1985. doi: 10.1109/TBME.1985.325509. [Online]. Available: <http://ieeexplore.ieee.org/document/4121989/> [Page 21.]
- [33] H. R. Wilson and J. D. Cowan, “Excitatory and Inhibitory Interactions in Localized Populations of Model Neurons,” *Biophysical Journal*, vol. 12, no. 1, pp. 1–24, Jan. 1972. doi: 10.1016/S0006-3495(72)86068-5. [Online]. Available: <https://linkinghub.elsevier.com/retrieve/pii/S0006349572860685> [Page 22.]
- [34] C. M. Schirmer, J. L. Shils, J. E. Arle, G. R. Cosgrove, P. K. Dempsey, E. Tarlov, S. Kim, C. J. Martin, C. Feltz, M. Moul, and S. Magge, “Heuristic map of myotomal innervation in humans using direct intraoperative nerve root stimulation,” *Journal of Neurosurgery: Spine*, vol. 15, no. 1, pp. 64–70, Jul. 2011. doi: 10.3171/2011.2.SPINE1068. [Online]. Available: <https://thejns.org/view/journals/j-neurosurg-spine/15/1/article-p64.xml> [Page 24.]
- [35] J. R. McIntosh, E. F. Joiner, J. L. Goldberg, L. M. Murray, B. Yasin, A. Mendiratta, S. C. Karceski, E. Thuet, O. Modik, E. Shelkov, J. M. Lombardi, Z. M. Sardar, R. A. Lehman, C. Mandigo, K. D. Riew, N. Y. Harel, M. S. Virk, and J. B. Carmel, “Intraoperative electrical stimulation of the human dorsal spinal cord reveals a map of arm and hand muscle responses,” *Journal of Neurophysiology*, vol. 129, no. 1, pp. 66–82, Jan. 2023. doi: 10.1152/jn.00235.2022 [Page 24.]
- [36] M. Sonoo, “Recent advances in neuroanatomy: the myotome update,” *Journal of Neurology, Neurosurgery & Psychiatry*, pp. jnnp–2022–329696, Jan. 2023. doi: 10.1136/jnnp-2022-329696. [Online]. Available: <https://jnnp.bmj.com/lookup/doi/10.1136/jnnp-2022-329696> [Page 24.]
- [37] L. H. Phillips and T. S. Park, “Electrophysiologic mapping of the segmental anatomy of the muscles of the lower extremity,” *Muscle & Nerve*, vol. 14, no. 12, pp. 1213–1218, Dec. 1991. doi:

10.1002/mus.880141213. [Online]. Available: <https://onlinelibrary.wiley.com/doi/10.1002/mus.880141213> [Page 24.]